Thesis

EXPLORATORY PROCESS-BASED MODELLING OF ESTUARINE SAND DUNES

The influence of environmental and empirical model parameters on expected wave lengths, growth rates and migration rates

May 12, 2022

Dieuwke Saskia Maas
S1562800
Civil Engineering and Management with profile River and Coastal Engineering
Department Water Engineering and Management
University of Twente
d.s.maas@student.utwente.nl

Colophon

This document is a Master Thesis to obtain a Master of Science in Civil Engineering and Management at the University of Twente.

Title: Exploratory process-based modelling of estuarine sand dunes: The influence of environmental and empirical model parameters on expected wave lengths, growth rates and migration rates
Author: Dieuwke Saskia Maas
Student Number: S1562800
Email: d.s.maas@student.utwente.nl

Version: Final version
Date: 12-05-2022
Date of presentation: 20-5-2022

University: University of Twente
Drienerlolaan 5
7522 NB, Enschede
Faculty of Engineering Technology
Department of Water Engineering and Management

Graduation committee
Head of committee: Prof. Dr. S.J.M.H.Hulscher
Committee member: Dr. Ir. P.C. Roos
Daily supervisor: Ir. W.M. van der Sande

Abstract

Estuaries are large water bodies connecting river(s) with the seas. These areas form the transition between the fluvial situation in rivers to the marine processes at seas. These estuaries are important since the surroundings are highly populated and have both economical and ecological value.

In these estuaries, we find large-scale rhythmic bed forms named sand dunes. The sand dunes are formed on top of the flat bed, develop into dunes under local environmental conditions over time and can migrate. This development of sand dunes affects the water depth and flow of the estuary. However, these sand dunes form only at some locations in estuaries. To better understand the formation of sand dunes, this study analysis the initial formation of a sand dune based on local environmental parameters in the process-based linear stability model developed by van der Sande et al. (2021a). This study analyses the effect of a change of one or several of the input parameters. These affect the expected fastest growing mode (FGM), being growth rate, wavelength and migration rate.

This current model describes the formation of sand dunes including the estuarine processes, in the Gironde Estuary. However, this current model can adapt to different circumstances by changing the local environmental parameters and the empirical model parameters. Herein the environmental parameters are the water depth, depth-averaged M2 velocity amplitude, the depth-averaged river flow velocity, grain size and the salinity gradient. empirical model parameters consist of the drag coefficient, slip parameter, bed load exponent and slope correction factor. In this study, we analyse the effect of the local ranges in parameters on the expected FGM properties. Secondly, we look into the combined effect of combined changes in these parameters. The third step in this study is to validate the current model based on the three locations and their environmental parameters combined with measurements of local sand dunes.

The individual parameter changes have a different impact on the growth rate, wave length and migration rate. Combing all changes in the environmental parameters, we find large variations in migration rates and directions. While the combination of ranges in the model parameter mainly influences the range in growth rates and wave lengths. The combination of two parameters will influence the FGM properties different since some parameters influence each other. So influence the combination of the bed load exponent and the slope correction the amount of sediment transport in the equation. The slope correction factor has a large influence on the wave length, however both factors influence the expected growth and migration rates.

The current model helps to understand the formation and different sizes of sand dunes. But not all differences in wave lengths and migration direction could be explained by the

local parameters in this model. The model is calibrated for the Gironde Estuary and the slip parameter needs to be adjusted to better present the wave lengths at other locations, however the current model can explain some difference between wavelengths between some locations. But there is still some difference which could not be explained. Also the migration direction is not always in the expected direction due to the type of model and the input parameters. So the current model is relatively robust, however it can not explain all the differences in wave lengths and migration directions.

Preface

This thesis concludes the 'Civil engingeering and management' master programme at the University of Twente, with the profile 'River and Coastal engineering'. The research was conducted at the University of Twente related to the PhD of Wessel van der Sande on the topic of modelling estuarine dune formation.

I would like to thank all the members of my graduation committee for their commitment and feedback during my thesis work. A special thanks to my daily supervisors Wessel van der Sande for the meetings and advice, as well as the time invested in me.

Last, but not least, I would like to thank my family and friends for providing me their unconditional support during this master thesis and earlier in my studies. I hope you will enjoy reading this report.

Dieuwke Maas
Enschede, May 2022

Contents

1. Introduction

This chapter provides an introduction to the research done for my master thesis. It consists of a literature background. Secondly, the research goal is described and the research questions used to reach this goal. Lastly, this chapter provides a reading guide for the rest of the report.

1.1. Background

Estuaries are large bodies of water enclosed by land, which are the transitional zone influenced by the significant freshwater discharge of rivers and the tidal influx of water by seas and oceans (Kennish, 2002; Adey and Loveland, 2007). The length of estuaries ranges between tens and hundreds of kilometres (Adey and Loveland, 2007). Estuaries are surrounded by highly populated land (Adey and Loveland, 2007; Leuven et al., 2019). Those humans use estuaries and their surrounding area for urban development, land reclamation, waste disposal, water extraction and diversion, agriculture and aquaculture, marine transportation and shipping, harbour and marina operations, and recreational and commercial fishing and therefore represent a very important economical and ecological value (Kennish, 2002).

Estuaries are influenced both by marine and fluvial processes. But they are also affected by estuarine-specific processes, like gravitational circulation. Dalrymple and Choi (2007) present a schematization of the influence of different types of energy on the marine and fluvial processes depending on the location of the estuary, presented in Figure 1. The effect of the tide is mainly on an area closer to the sea, while the river discharge has its main effect close to the river mouth. The measured tidal wave in estuaries is mainly asymmetrical (Berne et al., 1993; Schrottke et al., 2006; Vandenbruwaene et al., 2013). Guo et al. (2019) describes that the incoming tide is asymmetrical since the incoming marine tidal wave is a combination of an M2 wave, combined with an M4 wave. The incoming tidal wave is altered by the bottom friction (based on water current) and water depth (Dronkers, 1986; Dalrymple and Choi, 2007). The tidal amplitude can increase within an estuary based on the balance of bottom friction and channel width convergence. The name of the increase of tidal amplitude is hypersynchronous, the decrease of the tidal amplitude is called hyposynchronous (Dalrymple and Choi, 2007; Leuven et al., 2019).

1.1.1. Gravitational circulation

The gravitation driven estuarine circulation is the flow based on the difference in density between the fresh river(s) inflow and the denser saline water of the sea/ocean. At the estuarine mouth, there is an inflow of the dense shelf water below the outflow of the existing water mixture in the top layer of the water column. The higher density of the water causes this bottom inflow. The tides provide an inflow of saltwater that penetrate the estuary. The difference in density and the salinity gradient separates the two fronts. However, the

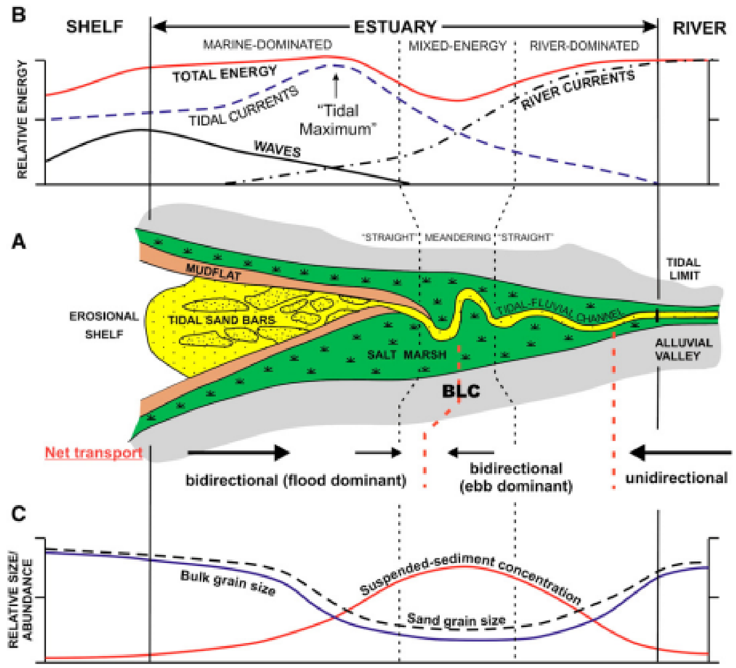

Figure 1: Distribution of the energy and sediment transport over the length of the estuary (Dalrymple and Choi, 2007)

flow of the river and tide creates shear stresses between the two different water mixtures. Mixing takes place between both fronts, as shown in Figure 2. With large river inflows compared to the tidal inflow less, mixing takes place. With large tides, a well-mixed estuary forms with brackish water. The horizontal salinity gradient is used to describe the amount of mixing of both flows within the estuary. This salinity gradient is the amount of change in the salinity over some length of the river. River floods interfere with the existing balance within the estuary, due to a large inflow of freshwater which flushes out the present existing balance of brackish water (Colling et al., 1999; Geyer and MacCready, 2014).

1.1.2. Bed forms

One of the processes in estuaries (and other water bodies) is the formation of bed forms. These bed forms can be explained due to the morphological loop. This loop explains that the hydrodynamics effect the amount of sediment transport. So differences in the hydrodynamics can results in some difference in the sediment transport. If the sediment transport is effected it, can deposit or erode the bed which are in morphological alterations.

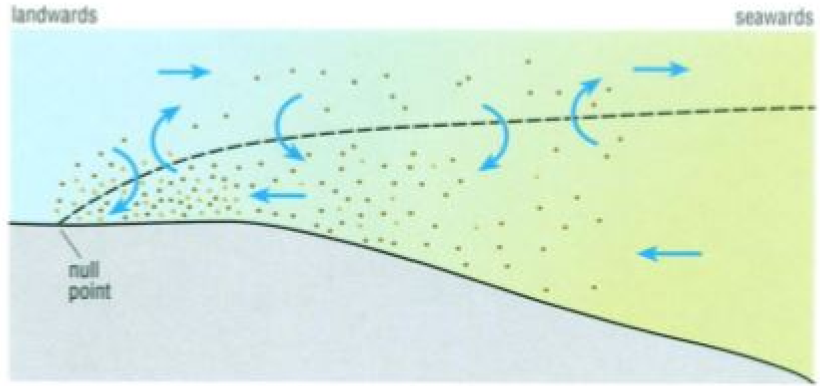

Figure 2: Schematization of the density-driven estuarine circulation. The flow represented on top part of the watercolumn is the freshwater flow and the saltwater flow is represented by the lower part of the water-column. (Colling et al., 1999)

These alterations in the bed result in small changes in the hydrodynamics above this bed. This cycle is described in the morphological feedback loop. This loop helps to understand how the different parts in this loop effect each other. Also the loop help to understand the formation of bed forms. Since this loop can help in to explain the deposits of sediment around crests to increase this bed forms. There are different types of bed forms (partly classified by size) and locations (oceans/seas, estuaries and rivers). The large scale bed forms perpendicular to the main flow direction are compered in the paper of van der Sande et al. (2019). Those are marine sand waves, estuarine sand dunes and river dunes (located in seas, estuaries and rivers). Their crests are perpendicular to the main current. They all have significant longer wave lengths than water depths (Hulscher and Dohmen-Janssen, 2005). Figure 3 shows the processes of the hydrodynamics which help to form these bed forms.

1.1.3. Marine sand waves

Marine sand waves (also named tidal sand waves) are mostly symmetrical rhythmic patterns perpendicular to the tidal current (Terwindt, 1971). The sand waves occur in sandy areas of shallow seas (McCave, 1971). The most sand waves are found at locations with depths between 20 and 55 meters (Bijker et al., 1998). They characteristically have wave heights in the order of 1-10 meters (Bijker et al., 1998), however Ashley (1990) uses a minimum of 1 meters to classify it as a sand wave. The height of the sand waves is limited by the water depth (Bijker et al., 1998). The wavelengths range between 100 and 1000 meters (Bijker et al., 1998; van Dijk and Kleinhans, 2005; Damen et al., 2018), but different papers

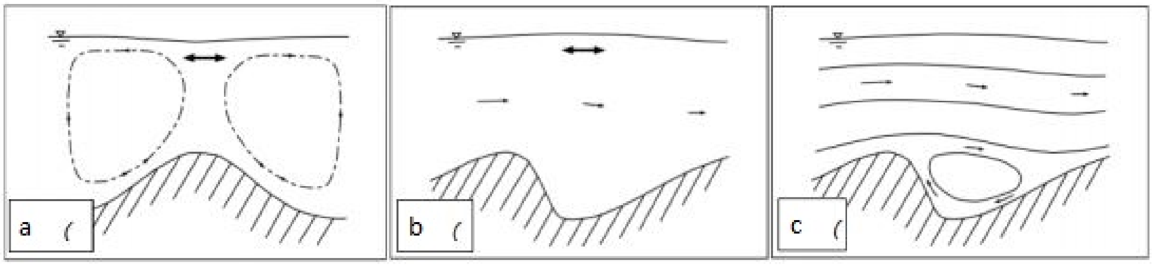

Figure 3: Schematization of the flow patterns and shapes of three different bed forms. *a* marine sand waves, which are driven by the tidal current. *b* estuarine sand dunes, which are affected by the tidal current and the river flow. However, this interaction is still not understood.*c* sketch of a river dune effected by the river flow including flow separation in the trough (van der Sande et al., 2019) inspired by Hulscher and Dohmen-Janssen (2005)

report a range of 200 to 500 meters (McCave, 1971) and 100 to 800 meters (Hulscher, 1996). The sand waves grow due to the residual vertical circulation caused by the tide. This tidal-averaged circulation effects the growth of sand dunes due to the flow from the trough to the crest and then goes up in the water column, which helps to transport sediment from the troughs to the crests (shown in Figure 3). Sand waves migrate due to a net transport into one direction due to both a residual current or an M4 wave (or higher orders) on top of the symmetrical M2 tidal wave (Nemeth et al., 2002; Besio et al., 2004). The migration rates vary for different locations, but also due to different temporal conditions, for example, storms (van Dijk and Kleinhans, 2005). The migration speeds ranges around tens of meters per year (Bijker et al., 1998; van Dijk and Kleinhans, 2005; Auguste et al., 2021) and Auguste et al. (2021) described a maximum value of 200 meters/year .

1.1.4. Estuarine sand dunes

Estuarine sand dunes (sometimes named estuarine sand waves) are large scale rhythmic sandy bed forms mostly perpendicular to the current (based on location more tide or river current) (Bokuniewicz et al., 1977; Colling et al., 1999). Ashley (1990) describes a typical estuarine sand dune in the order of 10 to 100 meters in length, however in this same paper, they give also an example of estuarine sand dunes in the Lougher Estuary, Wales with spacings between 75 and the 125 meters. Also Table 1 describes a maximum wavelength of 368 meters (Weser), but also much smaller sand dunes lengths of a minimum of 16 meters (Shuwei et al., 2016) . The wave heights vary between 0.6 meter (Western Scheldt) and 5.9 meter (Weser) based on the numbers in the Table 1. Some of the papers also report the migration speeds of the sand dunes. For example van Rijn (1993) reports migration on a daily basis, however Wienberg and Hebbeln (2005) report for a longer period. In Long Island Sounds the migration speeds vary between 35 and 150 meters per year (Bokuniewicz et al., 1977). However, those values variate per location and size of sand dunes. For example Zorndt et al. (2011) reports lower migration rates, which varies between the 24 and the 100 m/year.

1.1.5. River dunes

River dunes are large scale bed forms in the fluvial systems, influenced by the unidirectional flow of the rivers (Hulscher and Dohmen-Janssen, 2005) The dunes consist of silt to gravel, however are mainly found in sandy rivers (Best, 2005; Hulscher and Dohmen-Janssen, 2005). The river dunes are caused by the turbulence flow interaction with the sandy bottom(Warmink et al., 2014). Carling (1999) describes the dimensions of over 0.6 meters in length and wave height larger than 0.1 meters, so they are smaller than the estuarine sand dunes and marine sand waves. Based on field studies and laboratory experiments, researchers present relations between the water depth and the wavelength and wave height of river dunes (Allen, 1978; Bradley and Venditti, 2017). Bradley and Venditti (2017) describes a wavelength of 5 times the water depth and the wave height is one-sixth of the water depth with some maximum relation up to 1/2.5 of the water depth. In the past the focus of river dune studies was on the formation of river dunes develop during floods since this bed roughness influence the water levels during the flood (Warmink et al., 2014). The dunes grow faster due to increased discharges flow velocities and bed shear stresses. The maximum dimensions of these flood river dune are measured some time after the flood (Paarlberg et al., 2006). To understand the formation of the river dunes, laboratory experiments are conducted, here the growth rate is higher than for field observations since the time of growth during floods is limited. But the river dunes are also mobile during periods of lower discharges (Lokin et al., 2022). The wave lengths is typical in the order of ten times the height (Warmink et al., 2014), this wave length increase during the period after flood during mean discharges and low discharges of the river(Lokin et al., 2022). However Vittori and Blondeaux (2020) describes a much smaller wave length of the order of the depth of the river. The river dunes have higher migration rates than the marine sand waves and the estuarine sand dunes, in the order of several meters per day (Wilbers and Ten Brinke, 2003) instead of tens of meters per year.

1.1.6. Studies of bed forms

The formation and growth of these bed forms are studied following field, flume and modelling studies to understand the changes, these methods are general to understand the hydrodynamic interaction in water bodies, for example Gurnell (2014) describes these methods for the interaction of plants and the hydrodynamics in rivers. The first method are field studies. The set up of the studies can differ, based of the goal of the field observations. The first field observations mainly determent the size of the sand dunes and measured some of the local parameters: the sediment size and the flow velocity of the water. However nowadays the field observations take place over a period of time, so these different studies combined shows the changes in size and location and therefor it can study the migration and growth of the existing sand dunes (Zomer et al., 2021; Berne et al., 1993). The second method is the laboratory research. This laboratory research is mainly based on research in flumes. Herein the formation and migration of bed forms is research, in a controlled environment, to better understand the formation and interaction between physical processes. For example Blom et al. (2003) used this method to better understand the vertical sorting of sediment for bed forms and nonuniform sediment in rivers. These flume experiments give more insight in the processes and improves the existing formulas of processes around bed forms. The last method is process based modelling. This is divided in several types models, divided in a full 3D process based model (for example in Delft3D) and more simplified models (Hulscher (1996); van der Sande et al. (2021a): a linear stability analysis). Both models give insight in he formation of bed forms, the full 3D models are more based on one location. The simplified models give a larger possibility to compare effects of different input parameters, while the full 3D models give a in depth view of one location.

1.2. Model of van der Sande et al. (2021b)

This research uses the idealized process-based estuarine sand dune model of van der Sande et al. (2021a). This model is a 2DV model, which includes hydrostatic shallow water equations, a gravitation circulation due to a salinity gradient, a bed load sediment transport and bed evolution modelling. The model combines the water motion, sediment transport and bed elevation changes on the site. Both the water motion and the sediment transport are influenced by each other. Figure 4 shows a situation sketch of the model. Since this model is solved based on a linear stability analysis, only the initial growth is presented. Therefore the hydrodynamics is calculated based of perturbations. This changes changes in sediment transport based on no perturbations and therefore bed level. Based on the chosen solution the two parts of hydrodynamics and sediment transport of the model do not interact. The hydrodynamics is used to calculate the sediment transport and the bed level changes, however there is no second calculation of the hydrodynamics based on the new bed. So the effect of the changes of the bed after several years is excluded in the solution of the model.

Hydrodynamics

The model presents the hydrodynamics by its momentum and continuity balance. This momentum balance describes the existing energy within the system. The continuity balance prescribes that all water modelled stays in the model and therefore the changes in movement

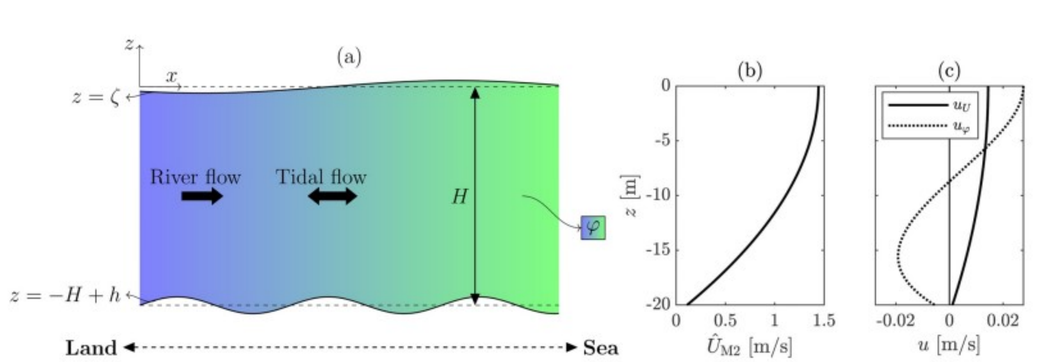

Figure 4: Overview of the model domain and an example of the solution of the basic state for the model (van der Sande et al., 2021a)

in one direction affects the water movement into another direction.

$$\frac{\partial u}{\partial t} + u\frac{\partial u}{\partial x} + w\frac{\partial u}{\partial z} = A_v \frac{\partial^2 u}{\partial z^2} - g\frac{\partial \zeta}{\partial x} - F_{btr}^{steady} - F_{btr}^{osc} - F_{bcl} \tag{1}$$

$$\frac{\partial u}{\partial x} + \frac{\partial w}{\partial z} = 0 \tag{2}$$

Equation 1 describes the momentum balance and Equation 2 the continuity balance. The black parts of the equations is the 2DV general hydrostatic shallow water equation (variant of the sand wave model of Hulscher (1996)) and the blue part of the equation represents the forcing terms of the hydrodynamics. F_{btr}^{steady} represents the river induced forcing, by a steady river inflow. F_{btr}^{osc} is the forcing by the tidal wave and F_{bcl} is the forcing based on the salinity-induced gravity circulation. In the general formula, u is the velocity in m/s split in a horizontal component u and a vertical component w. t is the time in seconds, x and z are the horizontal and vertical components in meters. A_v us the vertical eddy viscosity in m^2/s recalculated following $A_v = c_d H U_{M2}$ (Prandle, 1985). Herein is c_d the drag coefficient, H the mean water depth and U_{M2} the depth-averaged tidal velocity amplitude. g is the gravitation constant in m/s^2 and ζ the free surface elevation in meters.
This model has several boundary conditions, two at the water surface and two at the bed level.

The model imposes zero shear stress at the water surface, so all surface forces like wind are ignored. Also a kinematic boundary,condition exists which implies that all water particles stay part of the water body and therefore demand that the particles "follow" the water surface. And the author assumes that $Fr^2 = U_{M2}^2/(gH) << 1$ which removes the vertical water velocity at this boundary condition, therefore we can apply the boundary condition at $z = 0$, in equation 3.

$$\frac{\partial u}{\partial z} = 0, \qquad w = 0 \qquad at \qquad z = 0 \tag{3}$$

The two boundary conditions at the bottom describe the partial slip conditions and the kinematic conditions (Equation 4).Those are applied at the bed level at $z = -H = h$:

$$\frac{\tau_b}{\rho} = A_v \frac{\partial u}{\partial z} = su, \qquad w = u\frac{\partial h}{\partial x} \tag{4}$$

with τ_b the bed shear stress, ρ the water density (constant due to Boussinesq assumption) and s the slip parameter

Sediment transport equation

The sediment transport is described by the following Equation 5

$$q_b = \alpha_b |\tau_b|^{\beta_b} \left(\frac{\tau_b}{|\tau_b|} - \lambda \frac{\partial h}{\partial x} \right) \tag{5}$$

Herein is α_b is the bed load coefficient, τ_b the bed shear stress, β_b the bed load exponent, λ the bed slope parameter and h perturbation at bed level. In this equation the critical shear stress for the initiation of the sediment motion is ignored.

The two sub models (water motion and sediment transport) are coupled by the Exner equation presented in 6. This equation presents that the changes local changes in sediment transport affect the local bed level

$$(1-p)\frac{\partial h}{\partial t} = -\frac{\partial \langle q_b \rangle}{\partial x} \tag{6}$$

With p the average bed porosity, $\langle q_b \rangle$ is the tidal averaged sediment transport. This tidal averaged sediment transport is used, since during one tidal wave the sediment is transported in and out of the estuary, however the total change over one wave is responsible for changes in the bed and the formation of a bed form.

Linear stability analysis and results

These equations are the basis of the model solved through a linear stability analysis. In this linear stability analysis, the stability of the bed is investigated. The is achieved by analysing the response of the system to low-amplitude sinusoidal topographic perturbations. The basic state consists of a spatially uniform flow and sediment transport over a horizontally flat bed. The perturbed state consists of small-amplitude perturbations on the bed topography. This is formulates following $h = h_0 + h_1$ which h_0 =0 and $h_1 = \hat{h_1} exp(ikx) + c.c.$. This formulation is based on the assumption that the perturbed of the bed $\hat{h_1}$ is very small compared with the water depth (large values of the perturbation influence the hydrodynamics more than currently included and can not be solved following the linear stability analysis with $\hat{h_1}/H = \varepsilon$).This formulation of the bed influence the system φ and is dependent of several parameters, namely h, u, w, ζ, τ_b and q_b. This system is expanded in powers by ε.

$$\varphi = \varphi_0 + \varepsilon\varphi_1 + \mathcal{O}(\varepsilon^2) \tag{7}$$

In this equation is φ_0 the basic state and φ_1 the perturbed state, $\mathcal{O}(\varepsilon^2)$ represents the error of the system by excluding the higher-order terms because of a small ε. Also all individual parameters in this model are divided in a part representing their value during the basic state and one part presenting the perturbed state(example $u = u_0 + u_1$).

The basic state consist of a flat bed. The expressions of the basic flow and sediment transport are found by integrating the model equations and applying the boundary conditions. For the horizontal water motion we find a u_0 consisting of 3 terms: $u_0 = u_{0,bcl} + u_{0,btr}^{steady} + u_{0,btr}^{osc}$, this corresponds with the 3 forcing terms in Equation 1. In this formulated basic state we find some sediment transport, however this has no bed evolution as a result.

The perturbed flow and sediment transport are found through integration of the model equations. Based on the Exner equation (Equation 6 we could derive a growth equation based on the bed amplitude. $\frac{d\hat{h}_1}{dt} = \gamma\hat{h}_1 \rightarrow \hat{h}_1(t) = \hat{h}_{init}exp(\gamma t)$. This growth rate γ is a complex number($\gamma = \gamma_r + i\gamma_i$), the real part represents the growth of the sand dune amplitude height and the imaginary part can be described as a migration rate ($c_{mig} = -\gamma_i/k$), which represents the movement of the initial sand dune. If the is a positive growth rate for γ_r, for at least one wave number k, the flat bed is unstable and bed forms will develop. Since the current system is now applied for estuarine sand dunes, not all values of the wave number k are implemented, since there is no interest in studying the smaller bed forms.

The model can be used for several purposes, for example predicting the initial behaviour of a sand wave under local conditions. Then the model can present a growth curve (growth rate based on wave length or wave number) of the local circumstances and its corresponding migration rates. The maximum growth rate and its corresponding wavelength and migration rate is called the Fastest Growing Mode (FGM). Due to the highest growth rate, it is assumed that this is the mode preferred by the system, and this FGM is the wave length that matches the field observations at the location of the data. Another purpose is to get insight into the effect of changes in one individual parameter in the model on the outcome. In this case the outcome could be presented as a 3D graph, based on wave number, growth rate and the individual parameter. However those graphs are hard to read, therefore instead of the growth curve for each value of the individual parameter, we used the FGM and the corresponding values to present this growth curve. This gives a 2D graph with the range of the individual parameter and the FGM. Those parameters give an impression of which changes in dune size will be expected if one parameter changes. Currently the model is calculated in Matlab based on a range in wave number. This range in wave number represents the range in wavelengths calculated in the model.

1.3. Research goals

Currently van der Sande et al. (2021a) used his model to look into the effect of the gravitational circulation. Since he applied this extra part for the hydrodynamics, this also effect the influences of the different parameters. Currently the model is only applied to one site at the Gironde Estuary and used for only these parameters, however the environment and therefore some forcing is different in other estuaries .

The research aim is to better understand the formation of estuarine sand dunes. Herein, the parameters of sand dunes and the processes of the formation of sand dunes are important. Specifically, to what extent can the model of van der Sande et al. (2021a) be used to learn about the formation of estuarine sand dunes for typical values of estuaries. And what effect have individual parameters on the predictions of sand dune sizes and growth and migration of these sand dunes. And whether this model, created and calibrated for the Gironde estuary is suitable to be used for other estuaries. To achieve this research aim, the study is divided into the following sub-questions:

1. What are realistic values for model parameters used in the model for estuaries with sand dunes ?
2. What are the effects of one individual parameter changes on the fastest growing mode ?
3. What is the combined effect of varying the environmental or empirical model parameters of question 2 on the fastest growing mode and its corresponding migration rate?
4. How representative is the sand dune model of van der Sande et al. (2021a) with its current values for the Elbe and Scheldt estuary?

1.4. Reading guide

The current chapter explained the background and the research goals. Chapter 2 describes the methodology of this study. Chapter 3 researches the ranges in the input parameters within the model. These parameter ranges are implemented in the model in Chapter 4. Chapter 5 describes the range in outputs of combining all environmental parameters compared with combining all model parameters. The current model is validated in Chapter 6. The study presented in these chapters is discussed in Chapter 7. Chapter 8 is the conclusion of this study.

Table 1: Characteristics of some sand dunes in estuaries

Estuary	**Location**	**Wave length [m]**	**Wave height [m]**	**Depth [m]**	**Migration**	**Source**
Elbe	Hamburg	20-24	0.8-1.2	14.4	0.3m/day flood direction (downstream) and 0.3 m/day ebb direction	van Rijn (1993)
Elbe	Scharhörn	109-119	2.8-3.3	22	-	van Rijn (1993)
Elbe	Close to Hamburg	40-50, mean 46	1.8 (range 1.3-2.5)	Around 18	0.150 m/day downstream	Zorndt et al. (2011)
Elbe	Grauerort	20-38 mean 30	1.3-2.2 mean 1.7	20		Muurman (2021)
Gironde	Royan	37-182 mean 84	1.5-6.7 mean 4.9	20-30	Downstream crest migration	Berne et al. (1993)
Weser	Outer Weser	111-236 max 368	2-4.2 max 5.9	10-15	0.5-15 meters in 5 months downstream	Wienberg and Hebbeln (2005)
Weser	main navigation channel	max 150 mean 50	max 6 mean 2-3	14		Schrottke et al. (2006)
Western Scheldt	Vlissingen	155-330 mean210	1.7-3.4 mean 2.6	20-25		Muurman (2021)
Western Scheldt	Terneuze	30-120 mean 65	0.6-2 mean 1.25	35 max		Muurman (2021)
Western Scheldt	Borssele	60-220 mean 120	1.7-3.7 mean 2.5	10-25		Muurman (2021)
Western Scheldt	Raai E1 Zuidergat close to Vlissingen	mean 16	mean 0.66	10-25	-0.145 $m^3/m/day$ (ebb dominated sediment transport)	Vandenbruwaene et al. (2012)
Western Scheldt	Raai B4 Plaat Walsoorden close to Kloosterzande	mean 30	mean 1.46	10-25	0.165 $m^3/m/day$	Vandenbruwaene et al. (2012)
Yangtze	Bifurcation of South and North channel	15.9-58.8, 31.9 mean	0.67-2.47, 1.29 mean	13-17		Shuwei et al. (2016)

2. Methodology

The methodology describes the methods used to conduct the study. The first section explains some changes within the model of van der Sande et al. (2021b). The second section describes the search for realistic values of estuarine parameters. The third section describes the analyses of the effect of individual parameters. The fourth section describes the combined effects of or the environmental parameters of the model parameters. The fifth section describes the validation of the current model.

2.1. Model of van der Sande et al. (2021b) described in van der Sande et al. (2021a)

The idealized process-based estuarine sand dune model of van der Sande et al. (2021a) is earlier described in section 1.2. This current model is adjusted, so the recalculation of the vertical eddy viscosity is within the model and not only included as calculation of the input parameter and a sediment transport equation based on grain size and accuracy check in the perturbed flow model.

2.1.1. Sediment sizes

The sediment size is a crucial factor that affects the amount of bed load transport and suspended load transport. Currently, the model only uses parameters for bed load sediment transport, which partly depends on sediment size. Therefore the parameter α_{bed}, the bed load coefficient will be adjusted to calculated a valued depending on a uniform sediment size following van Rijn (1993, page 7.25 formula 7.2.44b) in the same method as Campmans et al. (2017).

The bed load coefficient in Equation 5 is a factor that scales the sediment in the correct order of magnitude. The value of α_b depends on several factors for example the sediment size and sediment and water density. The general equation of van Rijn (1993) is given by Equation 8

$$q_{b,c} = 0.1(s-1)^{0.5} g^{0.5} d_{50}^{1.5} D_*^{-0.3} T^{1.5} \tag{8}$$

With $q_{b,c}$ the volumetric bed load transport rate $[m^2/s]$ To calculate the volumetric bed load transport rate we use Equations 9 and 10 as sub calculations.

$$T = (\tau'_{b,c} - \tau'_{b,cr})/\tau'_{b,cr} \tag{9}$$

T is the dimensionless bed-shear stress, with $\tau'_{b,c}$ the effective bed shear stress (N/m^2) $\tau'_{b,cr}$ the critical bed-shear stress according to Shields (N/m^2)

$$D_* = d_{50}[(s-1)g/\nu^2]^{1/3} \tag{10}$$

D_* is the dimensionless particle parameter with d_{50} is the mean particle diameter (m), $s = \rho_s/\rho_w$ is the relative density, ρ_s is the sediment density (kg/m^3), ρ_w is the water density (kg/m^3), ν kinematic viscosity coefficient (m^2/s) and g is the acceleration of gravity (m/s^2) This "Van Rijn" bed load sediment transport formula (Equation 8) makes use of a critical shear stress, this critical shear stress is ignored in the sediment transport formula in the model. Also the "Van Rijn" equation excludes the effect of the slope, however this is included in the models of Campmans et al. (2017); van der Sande et al. (2021a). The "Van Rijn" bed load sediment transport formula (Equation 8) can be rewritten following the format of Equation 5 Equation 11 describes the formula of α following the format of Equation 5. This equation for α will be implemented in the model of van der Sande et al. (2021a), to include an uniform sediment sizes.

$$\alpha_b = 0.1(s-1)^{0.5} g^{0.5} d_{50}^{1.5} D_*^{-0.3} \tau_{b,cr}^{-1.5} \tag{11}$$

2.1.2. Accuracy check in the perturbed flow

The solution of the perturbed flow in the model of (van der Sande et al., 2021b) is found by numerically solving of their equations. Not all solutions found by the model based on this numerically solving present the system accurately. Therefor the accuracy of the perturbed flow model is evaluated based on the boundary conditions at the bed level (Equation 4). Due to the numerically solving and the program used not all parameters are exactly calculated. So when the bed level boundary conditions of the flow model are checked, if the error within these calculations is limited. With a limited error in these boundary conditions, the flow model is accurately calculated and therefore this solution can be used for the calculations of the sediment transport. In the case of an inaccurate solved perturbed state flow, the calculated sediment transport is an over-or under-estimation of the real transport and therefor the FGM properties and therefore the outcome is less relevant following the current solved perturbed state. Based on the outcome and use of the model this accuracy needs to be differently handled.

2.2. Realistic parameter values of estuaries

The first question is to find realistic values for parameters in the model. A literature study will provide these representative values. Herein we look at the ranges for the following parameters:

1. Water depths
2. Tidal velocity (M2 wave)
3. Depth-averaged river discharge
4. Salinity gradient
5. Sediment sizes

6. Vertical eddy viscosity and drag coefficient
7. Slip parameter
8. Bed load exponent in the sediment transport equation
9. Slope correction factor in the sediment transport equation

The first 5 parameters are classified as the environmental parameters. The last 4 parameters and excluding the eddy viscosity (this parameter depends on other parameters) are classified as empirical model parameters. Those parameters are chosen since they are input parameters for the model of van der Sande et al. (2021b) and vary based on locations and sediment transport model. For the environmental parameters, five estuaries are studied to represent a range, these are the Elbe, Gironde, Weser, Western Scheldt and the Yangtze estuary. The parameter values change within the estuary due to local differences. Also, the empirical model parameters are studied. Some of the empirical values depend on the sediment transport model while the drag coefficient and slip parameter vary based on location and how they are computed. So the general ranges of the values are described based on the literature study and if possible specific for the above named estuaries. The nine model parameters are important for research questions 2, 3 and 4.

2.3. Model output sensitivity due to individual parameters

The second research question contains nine sub-parts depending on the 9 different input parameters. In this sensitivity analysis, the nine model parameters are interesting.
The method used is one factor at the time (OFAT) sensitivity analysis. This analysis uses a base (default) set of parameters, in this case, the values of the Gironde estuary used by van der Sande et al. (2021a). For each sensitivity analysis, one parameter is varied, while we fix all other parameters on the Gironde values used in van der Sande et al. (2021a). Therefore the local effects of this parameter on the output is investigated, since the effect could be different with another base set of parameters.
The OFAT is used to explore the influence of all parameters. For each analysis, we pick 20 values linear between the minimum and the maximum values found in research question 1, except if there is another distribution of values found in the literature. Chapter 3 describes the range in parameters. The base model setting of the wave number ranges from 0 to 0.17 m^{-1}. The maximum wave number can increase if the range in wave number is too small. However the perturbed flow still needs to be accurate calculated. So a balance is found between the maximum value of the wave number, k and the accuracy of the solved perturbed states.
In this sensitivity analysis is the outcome, the change in the growth rate of the FGM, its migration rate and wavelength. Three figures present the results of each parameter, with on the x-axis the varied parameter and on the y axis its effect on the FGM its growth rate, migration rate and wavelength.

2.4. Effect environmental parameters compaired with the effect of empirical model parameters

Research question 3 consists of a comparison of the model and the environmental parameters. We split the sensitivity analysis into two global sensitivity analyses. One for the environmental parameters in the model and one sensitivity analysis for the model parameters. These parameters change according to the minimum and maximum values of research question 1 with a few small changes due to possible inaccurate calculations. For example, the model parameter of the bed load exponent is limited since this parameter has a large impact on the sediment transport, however with changes of the bed load exponent β_b also the bed load coefficient, α_b changes within the sediment transport equation, however this correlation between those parameters is not included in the model. This solution gives a variation due to local measurements and the calibration range of the model parameters.

The outcome of this sensitivity analysis is a distribution of the FGM growth rate, its wavelength and its corresponding migration rate. Three histograms will represent those distributions based on accuracy and a wavelength within the range of sand dunes (so a maximum of k=0.17 m^{-1}).

2.5. Validation of the model

The idealised process-based sand dune model of van der Sande et al. (2021a) gave a range of sand dunes depending on variations of estuaries. Research question 3 presents the possible variations of sand dunes following the model. Currently, van der Sande et al. (2021a) calibrates the model for the Gironde Estuary. However, the model only represents this physical situation, so validation is needed to compare the modelled results with sand dune characteristics in other estuaries. Therefore three case studies will be performed for the Western Scheldt estuary (locations Vlissingen and Terneuzen) and the Elbe estuary (data available by Muurman (2021)). For both estuaries, we implement the local environmental parameters. In the case of the Scheldt estuary, Muurman (2021) looks at 3 sites where the site located at Vlissingen is relatively different from the sites located at Borssele and Terneuzen. Since the forcing in Borssele and Terneuzen are comparable and almost have the same wave length we only use two sites at the Scheldt(Vlissingen and Terneuzen) and only one site in the Elbe. The first check is to implement the environmental parameters and compare the model calculated FGM wave length and migration with the expected wave length measured in the estuary. Based on this analysis, the slip parameter will be re-calibrated based on the wavelength on these new locations. If the slip parameter has small changes, the model is robust and can be easily applied for predictions of other estuarine sand dunes.

3. Realistic parameter values of estuaries

This chapter looks into the variation of the different input parameters in the estuarine sand dune model of van der Sande et al. (2021a). This model uses the water depth, tidal and residual current, sediment size and salinity. To find realistic estuarine values for these parameters, we use the parameter values of five estuaries: the Elbe, Gironde, Weser, Western Scheldt and the Yangtze estuary. The Gironde is an estuary in France. The Elbe and the Weser estuary are in Germany. The Western Scheldt locates in The Netherlands. The Yangtze is the largest estuary in China, also named the Changjiang estuary. Also, this chapter researches the variation of the drag coefficient (or vertical eddy viscosity), the slip parameter, the bed load exponent and the slope correction factor. The following chapters use these properties as input parameters.

3.1. Water depth

The model water depth described is the mean local water depth, so tide average and excluding the effect of bedforms on local water depths. The water depth of the Elbe estuary is 22 meters at the mouth near Scharhorn. This water depth decreases to a water depth of 14.4 meters near Hamburg (van Rijn, 1993; Papenmeier, 2012). The Gironde has water depths of 30-35 meters in the channel close to the sea after the two channels merges (Berne et al., 1993). The Weser estuary has water depths of 6-20 meters (Wienberg and Hebbeln, 2005), Grabemann et al. (1997), however, describes that the outer estuary has an average depth of 16 meters and the inner estuary depth of 12 meters. The Western Scheldt has a water depth of 15 meters at Vlissingen and decreases to 3 meters at Gent (Sistermans and Nieuwenhuis, 2021). The Yangtze estuary has water depths ranging between 4.9 and 24 meters (Wu et al., 2016b).
So the water depths vary within an estuary, especially between the upstream and downstream parts of an estuary. The Elbe and Western Scheldt have a greater depth close to sea than upstream. Also, Sistermans and Nieuwenhuis (2021) and Wu et al. (2016b) describe that the water depth in the navigation channels is maintained by dredging to maintain the current water depths and deepening it if needed. The water depths range between 3 and 35 meters for there five estuaries.

3.2. Tidal range and tidal current

Two parameters that describe the tide in an estuary are the range in tidal range and the tidal current.

3.2.1. Tidal range

The tidal range (difference between water level at ebb and flood is the same as twice the tidal amplitude) varies over the length of the estuary. Therefore several locations are used to describe the local tide. For example, the tidal range for the Elbe estuary is 3.0 meters at Cuxhaven (near the mouth of the estuary) and 2.7 meters at Glückstadt and 3.5 meters at Hamburg (around 90 km upstream) (Papenmeier et al., 2014). The tidal range of the Gironde is 1.3 to 5 meters at the estuary mouth during neap and spring tide (Allen and Castaing, 1973; Billy et al., 2012) and this tidal range increases to 3 to 6 meters at Bordeaux (Billy et al., 2012). The outer Weser has a tidal range of 3.5 meters (Wienberg and Hebbeln, 2005). The Western Scheldt has a tidal range of between 3.5 (Vlissingen at mouth of estuary) and 5.2 meters (Antwerpen upstream of Vlissingen) (Sistermans and Nieuwenhuis, 2021; Francken et al., 2004). The tidal range of the Yangtze estuary is 2.7 meters at the mouth and decreases upstream to Gaoqiao (2.4m) and Wusong (2.2 m) (Wu et al., 2016b). The tidal range depends on the estuary and the location within the estuary. The highest tidal range is 6 meters at Bordeaux. The smallest tidal elevation range found is 1.3 meters during neap tide at Royan. Both extremes are for the Gironde.

3.2.2. Tidal current

The tidal current or the tidal flow is the velocity created by the in- and outgoing tide. The ebb and flood current values differ due to tidal asymmetry. So, one tide is shorter in time and has a stronger tidal current than the other tide.
For example, the Weser is ebb dominant Schrottke et al. (2006) and Vandenbruwaene et al. (2013) describe that the time-averaged ebb and flood flow velocities range between 0.1 and 0.6 m/s. Vandenbruwaene et al. (2013) their figures suggest that the time-averaged flood flow velocity varies between 0.1 and 0.9 m/s depending on location. The time-averaged ebb flow velocity varies between 0.1 and 0.6 m/s over the length of the estuary. However, Schrottke et al. (2006) describes the mean tidal current of 1-1.3m/s, which is higher than the values described by Vandenbruwaene et al. (2013).
Muurman (2021) describes the current velocity of the Elbe Estuary by the time-averaged velocity amplitudes for the Pagensand Nord and the Rhineplate Nord. The average velocity amplitude at the Pagensand Nord is at bed 1.0 m/s and the surface 1.3 m/s, for the Rhineplate Nord is at bed 0.8 m/s and the surface 1.2 m/s. Vandenbruwaene et al. (2013) show that the mean tidal current varies over the length of the estuary between 0.2 and 0.9 m/s with stronger flood currents than ebb currents.
For left flank close to the mouth of the Gironde estuary, Berne et al. (1993) describes a peak ebb current of 98 cm/s and a peak flood current of 88 cm/s during spring tide, these peak currents decrease to a tidal current of 50 cm/s for both ebb and flood during the neap tide.
Vandenbruwaene et al. (2013) studies the Western Scheldt, where the mean tidal velocities vary between 0.1 and 1 m/s depending on the location. But Muurman (2021) suggest a higher tidal current with a velocity amplitude of 1.3 m/s close to Vlissingen, this tidal current decreases to 1.1 m/s for Borssele and Terneuzen. However, Sistermans and Nieuwenhuis (2021) suggest even a higher tidal current of 1 to 2 m/s in the main channels.
The Yangtze has a mean tidal velocity of 1 m/s (Hu et al., 2009). Wan et al. (2014) measures

Estuary	Mean discharge m^3/s	Maximum discharge m^3/s	Minimum discharge m^3/s	Area cross-section m^2 [a]	U_{res} mean m/s	U_{res} max m/s	U_{res} min m/s
Elbe	325 [b]	1920 [c]	278 [c]	3.2*10^4	0.010	0.060	0.0087
Gironde	900 [d]	5000 [e]	160 [e]	8.0*10^4	0.011	0.063	0.0020
Weser	713 [f]	1230 [g]	118 [g]	9.5*10^3	0.075	0.13	0.012
Western Scheldt	107 [h]	191 [i]	78 [i]	2.7*10^4	0.0040	0.0071	0.0029
Yangtze	$2.93 \cdot 10^4$ [j]	$7.71 \cdot 10^4$ [k]	$1.17 \cdot 10^4$ [k]	1.5*10^5	0.20	0.51	0.078

Table 2: The calculated residual current. [a]: Appendix A [b]: Grabemann et al. (1997) [c]: Papenmeier (2012) [d]: Berne et al. (1993) [e]: van Maanen and Sottolichio (2018) [f]: Papenmeier et al. (2014) [g]:Schrottke et al. (2006) [h]: Francken et al. (2004) [i]: Damme et al. (2005) [j]: Wu et al. (2016b) [k]: Weihua et al. (2008)

a tidal-period and depth-averaged value of the flood tide between 0.3 and 1.2 m/s. The ebb tide varies between 0.6 and 1.7 m/s. Wan et al. (2014) took those measurements between Xuliujing (before the bifurcations) and Niupijoa (in the North Passage).

So to conclude, the values vary between measurements (in time and location) in an estuary and between different estuaries. The ebb and flood current velocities differ within an estuary. The lowest current velocity is a local mean velocity of 0.1 m/s, found in the Weser and at the Western Scheldt Estuary. The highest suggested tidal current is 2.0 m/s for the Western Scheldt.

3.3. Residual current

The residual current is the effect of the river discharge on the estuary. This residual current will be calculated.

$$U_{res} = Q/A \tag{12}$$

With U_{res} the residual current in m/s, Q the river discharge in m^3/s and A the surface area of the cross-section in m^2. Table 2 shows the calculation of the residual current. Appendix A explains the values calculated for the surface area A. Here the mean, low and high discharges are used to give a range in the residual current of each estuary.

The values of the discharge and residual current of the Yangtze estuary are significantly higher compared with the values of other estuaries. The Gironde Estuary has the lowest values of 0.0020 m/s, and the highest value is found for the Yangtze estuary and is 0.51 m/s. All river currents have values between 0 and 0.05 m/s except for the Yangtze, which has a value of 0.2 m/s.

3.4. Sediment size

The grain size described is a mean grain size used at locations with sand dunes. The grains are mostly sand, but there are findings of fragments of clay and silt at sand dunes. The mean sediment size of the Elbe estuary is in the range of 300-500 μm following van Rijn (1993), this corresponds with the values of 343-478 μm with a mean value of 407 μm described by Muurman (2021). In the Gironde a wider mean sediment size range is found of between 320 and 650 μm, so this is mean to coarse sand (Berne et al., 1993). In the Weser estuary, sand dune grain size is coarser with mean values of between 350-490 μm following (van Rijn, 1993) and 200-700 μm following (Herrling et al., 2021). The Western Scheldt has a sediment size of 150-300 μm in the navigation channel, and this decreases to smaller than 200 μm for the shoals (Sistermans and Nieuwenhuis, 2021). Francken et al. (2004) describes a larger sediment size variation of 100-700μm, while Muurman (2021) describes larger sediment size than Sistermans and Nieuwenhuis (2021) of 237-406 µm with a mean value of 294 μm. The Yangtze estuary has a smaller sediment size of 8-170 µm (Wu et al., 2009) and a mean sediment size of 108 μm (Shuwei et al., 2016), so here the bed consists of silt and sand.
The sediment sizes range between the smallest mean sediment size in the Yangtze of 108 μm. And the largest sediment size ranges between 320 to 650 μm for the Gironde. For the Weser, the largest sediment size found equals 700 μm.

3.5. Salinity gradient

The salinity gradient describes the change in the salinity for one location or over a length. In general, we expect to find a salinity of 30 psu for seas and oceans. Freshwater has low salinity close to zero psu. The minimum salinity gradient is 0, so no change in salinity at this location or area. The Elbe estuary has a mean salinity gradient of 0.38 psu/km, which differ between local seasonal values of 0.11-0.60 (Vandenbruwaene et al., 2013). The Gironde Estuary has a salinity between 0.1 and 0.6 psu/km (van Maanen and Sottolichio, 2018). However, van der Sande et al. (2021a) presents a range of 0 to 1.3 psu/km based on the same paper of van Maanen and Sottolichio (2018). The mean salinity gradient of the Weser is 0.43 psu/km (Vandenbruwaene et al., 2013). The Western Scheldt has a mean salinity gradient of 0.4 psu/km. This salinity gradient decreases to 0.35 psu/km for the summer. And has a local maximum of 0.57 psu/km in the winter (Vandenbruwaene et al., 2013). The Yangtze has a mean salinity gradient of 0.3 psu/km and local values of between 0.1 and 0.6 psu/km (Wan et al., 2014). van der Sande et al. (2021a) suggests the lowest and higehst salinity gradient and therefore the range for the salinity gradient of 0 and 1.3 psu/km for the Gironde estuary.

3.6. Vertical eddy viscosity and drag coefficient

The vertical eddy viscosity describes the turbulence transfer in the water column. The model of van der Sande et al. (2021a) uses a constant eddy viscosity. In reality, the eddy viscosity changes over time and in the water column. van der Sande et al. (2021a) use a fixed vertical eddy viscosity of 0.05 m^2/s based on the formula $A_v = c_d H U_{M2}$, with c_d (the drag coefficient) of 0.0025. More papers describe the eddy viscosity in estuaries. For example, Wei et al. (2016) uses a vertical eddy viscosity of 0.0085 m^2/s for the Scheldt Estuary and uses the range of 0.001 and 0.1 m^2/s for a sensitivity analysis. de Jonge et al. (2014) describe that the eddy viscosity coefficient differ over the years for the Ems Estuary, which varies between 0.011 and 0.18 m^2/s, but Chernetsky et al. (2010) only suggest 0.019 m^2/s for 1980 and 0.012 m^2/s for 2005. Those values are higher than found by de Jonge et al. (2014). Schramkowski and de Swart (2002) suggest that the values differ between locations within the estuary. They obtain realistic values for the vertical eddy viscosity parameter between 0.062 and 0.207 m^2/s for the Western Scheldt with an average of 0.096 m^2/s.
Also, the drag coefficient can describe the vertical eddy viscosity. The drag coefficient varies over time and width and is case depending (Ullman and Wilson, 1998; Li et al., 2004). Prandle (1985) uses a drag coefficient of $2.5*10^{-3}$ however others describe a higher range of $2.5*10^{-3}$ to $1.0*10^{-2}$ (Ong et al., 1994) or even $5.0*10^{-3}$ to $2.0*10^{-2}$ for sinuous estuaries (Bo et al., 2021). But Lu et al. (2019) describes lower drag coefficients mean values of $1*10^{-3}$ and $8*10^{-4}$ for the North Passage in the Yangtze River estuary during a few days. But these measurements are local and only for a short time. Lyu and Zhu (2018) shows a bottom drag coefficient in the range of $1.5*10^{-3}$ to $4.3*10^{-3}$ for the Yangtze estuary.
The analysis describes a vertical eddy viscosity parameter between 0.0085 and 0.21 m^2/s. This range is almost within the lower range for coastal sand dunes suggested by Hulscher (1996) which is 0.01-0.5m^2/s. However, the estuarine values are significantly higher than the river dune value of $1.9 \cdot 10^{-4} m^2/s$(Paarlberg et al., 2006). The drag coefficient ranges between $8*10^{-4}$ and $2.0*10^{-2}$.

3.7. Slip parameter

To slip parameter (alias resistance parameter), determines the relation between horizontal velocity and the shear stress on top of the boundary layer at the bed level (Hulscher, 1996). Currently the model of van der Sande et al. (2021a) uses a slip parameter of 0.04 m/s based on a calibration. In theory the slip parameter can vary between no stress ($s \rightarrow 0$ m/s) and no-slip, which results in infinity stress ($s \rightarrow \infty$ m/s) (Maas and Haren, 1987). However in physical environments these minimum and maximum slip values are not that extreme and hove a smaller range in values.
Wei et al. (2016) describes the influence of the slip parameters for an estuary model. Here in they use a range of 0.0001 to 0.1 m/s with 0.0099 m/s as the default value of the model.

Also, Schramkowski and de Swart (2002) describes the slip parameter, now for the Western Scheldt of 0.007 - 0.024m/s. de Jonge et al. (2014) describes the variation of the slip parameter over a period 1960-2005, the lowest and highest values are 0.06 and 0.47m/s. Chernetsky et al. (2010) also describes the Ems Estuary and has only values of 1980 and 2005 those are 0.098 and 0.049 m/s.
The slip parameter for estuarine sand dunes varies between 0.007 and 0.47 m/s. This is significant smaller than coastal sand dunes with a range of 0.1-10 m/s (Hulscher, 1996) Paarlberg et al. (2006) describes a slip parameter of $1.9 \cdot 10^{-4}$ for river sand dunes. The estuarine slip parameter values are between the coastal sand wave and river sand dune slip parameter.

3.8. β_b: Bed load exponent

The values of the bed load exponent depend on the source and formula used. The transport formula depends on grain size and flow velocity (or shear stress) but not on the environment. Hulscher (1996) describes a similar formula for the sediment transport of sand waves and suggests that the bed load exponent varies between 1 and 3 and uses 1.5 in her model. However Campmans et al. (2017) suggest that typical values of the bed load exponent have a smaller range between 1 and 2 in his marine sand dune model. Also the formula of van Rijn (1993) (general sediment transport formula), the model of van der Sande et al. (2021a) (estuarine sand dunes) and Paarlberg et al. (2006) (river sand dunes) uses a the bed load exponent of 1.5. Based on this analysis, the bed load exponent will vary between 1 and 3. The most common value found is 1.5.

3.9. Bed slope coefficient

The bed slope coefficient includes the effect of a sloped bed. The bed slope varies due to sand dunes. A slope correction factor of 0 excludes the positive and negative influence of the bed slope on sediment transport. The current model of van der Sande et al. (2021a) currently uses a bed slope correction of 1.5. Baar et al. (2018) describes this slope correction factor, which can be calculated following several formulas, depending on sediment properties and fluid drag and sediment mobility. This paper only gives for one formula a fixed number of 1.1 for the equation of Wiesemann et al. (2006). Hulscher et al. (1993) suggest a correction rate of between 1-3 for coastal sand dunes for an equation depending on velocity, however in a later paper of her, she reports a correction rate of between 1 and 2 for a shear stress formula (Hulscher, 1996). Also the paper of Campmans et al. (2017) presents a range of between 1 and 2 for marine sand dunes. But Paarlberg et al. (2006) presents a significantly lower slope correction factor of 0.1 for river sand dunes. Both regimes influence the estuarine sand dunes so, the slope correction factor will range between 0.1 and 3.

3.10. Summery

Table 3 summaries all ranges for the found parameters.

Table 3: Overview of all ranges in parameters

Parameters	**Range**
Water depth [m]	3 -35
Tidal velocity [m/s]	0.1-2
River current [m/s]	0.002-0.51
Sediment size [μm]	108-700
Salinity gradient [psu/km]	0.0-1.3
Vertical eddy viscosity [m^2/s]	0.0085-0.21
Drag coefficient	$8.0*10^{-4}$ -2.0*10$^-$2
Slip parameter[m/s]	0.007-0.47
Bed load exponent [-]	1.0- 3.0
Bed slope coefficient [-]	0.1-3

Fra

4. Model output sensitivity due to individual parameters

The OFAT sensitivity analysis uses a base set and range of the variation per parameter needed. In this case, is the base set changes at the values of the Gironde Estuary used by van der Sande et al. (2021a). Table 4 presents the ranges and the values in the Gironde. For the base set, we find a growth rate of the FGM of 37/year . It has a wavelength of 100 meters and a landward migration rate of 94 meters per year.

Table 4: Parameter ranges found in research question 1

Parameters	**Default (Gironde)**	**Range**
Water depth [m]	20	3-35
Depth averaged M2 velocity amplitude [m/s]	1	0.1-2
River current [m/s]	0.011	0.002-0.51
Sediment size [μm]	-	108-700
Bed load coefficient, α_b [$m^{7/2}s^2$ $kg^{-3/2}$]	$1.56*10^{-5}$	recalculated based on D_{50}
Salinity gradient [psu/km]	1	0.0-1.3
Vertical eddy viscosity [m^2/s]	0.05	0.0085-0.21 (recalculated in the model)
Drag coefficient [-]	$2.5*10^{-3}$	$8*10^{-4}$ - $2*10^{-2}$
Slip parameter[m/s]	0.04	0.007-0.47
Bed load exponent [-]	1.5	1.0- 3.0
Bed slope coefficient [-]	1.5	0.1-3

4.1. Water depth

The water depth ranges between 3 and 35 meters depth, which results in a newly calculated vertical eddy viscosity between 0.0075 and 0.0875 m^2/s. Figure 5 shows the sensitivity of the variation of the total range. For the water depth larger than 26.5 meters the model has sometimes a perturbed flow calculated where the bed boundary conditions are inaccurately calculated, however, since the figure shows that the larger values follow an existing trend, the data can still give some insights into the effect of water depths larger than 26.5 meters. With a small water depth, the growth rate is high. This growth rate is inversely proportional, this is due to a smaller impact of some of the parameters on the bottom with larger depths. The wavelength of the FGM increases with a higher mean water depth. The smaller water depths causes a seaward migration. The migration is caused by the river discharge and the salinity gradient. The depth-averaged river discharge did not change in the model, however,

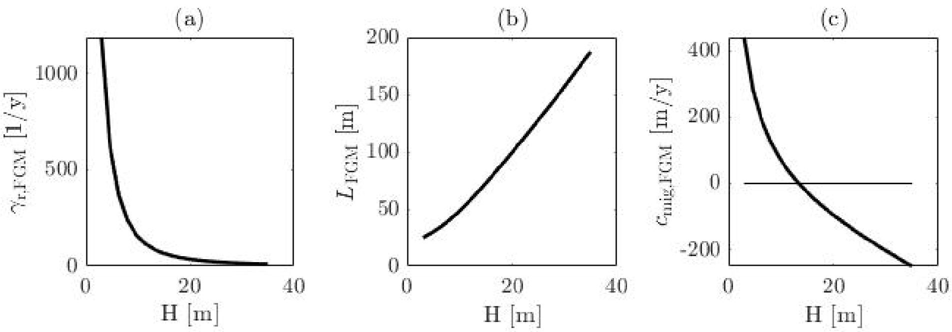

Figure 5: Sensitivity of the FGM to changes in the water depth range 3-35 (m) a: Growth rate of FGM b:wave length of FGM c: migration speed of FGM

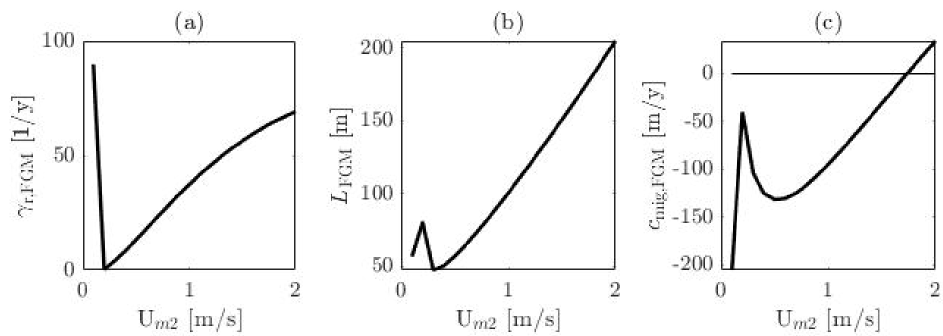

Figure 6: Sensitivity of the FGM to changes in the depth averaged M2 velocity amplitude range 0.1-2.0 (m/s), a: Growth rate of FGM b:wave length of FGM c: migration speed of FGM. The range 0.1 to 0.3m/s inaccurately calculated which causes the jumps in the graph

the salinity induced baroclinic forcing is affected by the water depth and therefore this effect increases with a larger water depth. The larger water depth decreases the bed stresses in the model, and the sand dunes can migrate upstream.

4.2. Depth averaged M2 velocity amplitude

The range for the depth-averaged M2 velocity amplitude is between 0.1 to 2 m/s. Therefore the vertical eddy viscosity varies between 0.005 and 0.1 m^2/s based on the changes in the depth-averaged M2 velocity amplitude that represents the tidal current. For the lowest values of the depth-averaged M2 velocity amplitude, the vertical eddy viscosity needs to be recalculated, since the river flow has also a large impact on the vertical eddy viscosity. This change is currently not implemented in the model. The increase of the tidal current affects the system since this increases the flow velocities and therefore the bottom friction and sediment transport. However, the tidal current also affects the eddy viscosity and therefore the calculation of the bed shear stress at the bed.

Figure 6 shows the results of the OFAT sensitivity of the tidal current. The first two points in the calculations are calculated, however, based on an inaccuraly calculated perturbed flow, therefore not all calculated values will have real meaning. So the steep part of the growth rate, the rapidly changes in the wave length and the steep parts in the migration rate at the lower values is probably due to an inaccurate calculation since they show a different pattern than the accurately calculated values. The maximum growth rate of 40/year is for a tidal velocity amplitude of 0.6 m/s and a wavelength of 63 meters. The wavelength of the fastest growing mode increases with an increasing tidal velocity amplitude. The maximum migration rate upstream is at a tidal velocity amplitude of 0.4 m/s and has a wavelength of 48 meters.

4.3. River current

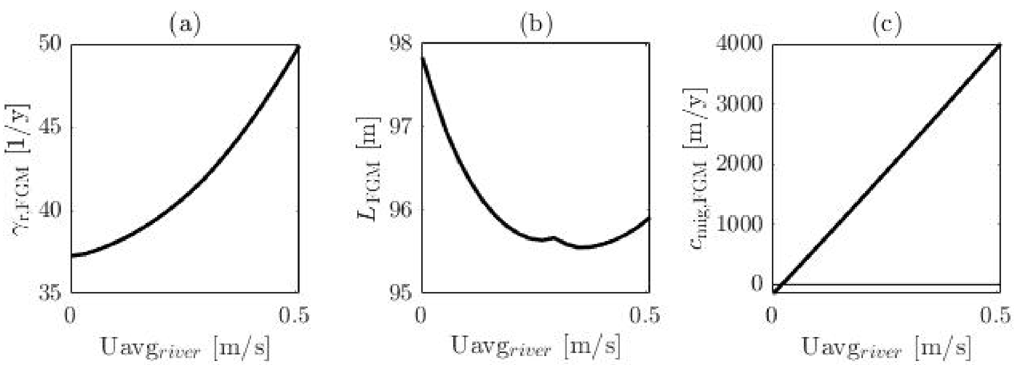

Figure 7: Sensitivity of the FGM based to changes in the river current range 0.002-0.51 (m/s) , a: Growth rate of FGM b:wave length of FGM c: migration speed of FGM

The river velocity varies between 0.0020 and 0.51 m/s. Figure 7 shows the results of the OFAT sensitivity analysis of the river depth-averaged current. When the river discharge increases, the growth rate of the FGM also increases, but the related wavelength has a minor decrease. The maximum growth rate is 49.9 for a river discharge of 0.51 m/s. The depth-averaged river current has an enormous impact on the migration rate of the FGM, with a maximum value of 4.0*10^3 meters per year (twice as high as migration of the median discharge in the Rhine (Lokin et al., 2022)). This impact could be expected since the river-current influence the asymmetry of the system and therefore creates a positive residual flow to the sea, which results in a positive migration speed in the direction to the sea.

4.4. Sediment size

The sediment size influences the alpha in the sediment model. Based on the recalculations of alpha for the sediment range of 108-700 *10^{-6} m this gives a α of 2.2*10^{-5}- 1.3*10^{-5} $m^{7/2}s^2$ $kg^{-3/2}$. The α_{bed} used as the base parameter is within the newly calculated range. Figure 8 shows some negative exponential relation between the sediment size and the new calculated α_{bed}. The increase in grain size decreases the α_{bed}.

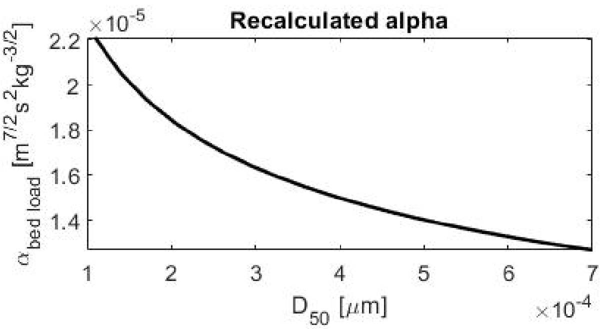

Figure 8: Recalculated alpha

Figure 9 describes the sensitivity of the sediment size. The growth rate decreases with decreasing alpha and increasing sediment size. The migration rate also increases (however the absolute migration decreases) with an increasing sediment size. The maximum growth rate is always found for the same wavelength, however the the growth rate at this location depends on the sediment size. We could have expected a trend of "a decreasing growth rate and migration rate for an increasing sediment size" since smaller sand grain sizes can be easier transported when the model excludes the suspended sediments. The model explains this decrease, since the larger grain sizes have a smaller alpha, which is a scaling parameter in the sediment transport equation, and since the alpha decreases, the amount of sediment transport decreases. This decrease in sediment transport is shown in the graph of the growth rate and migration rate.

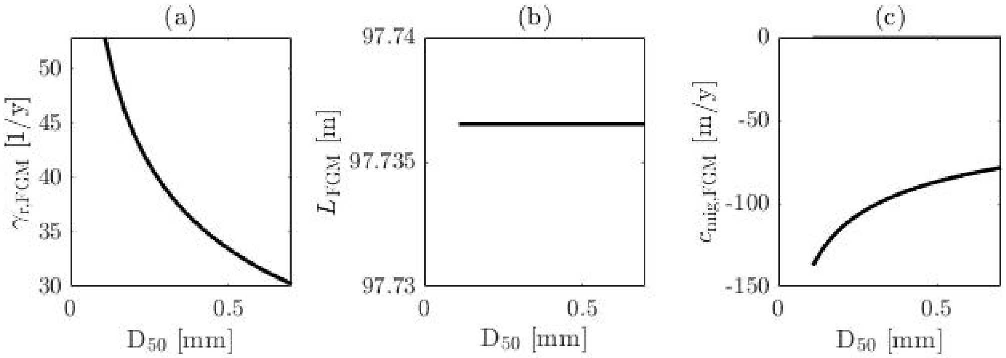

Figure 9: Sensitivity of the FGM to changes in the sediment size 108-700 (μm) , a: Growth rate of FGM b:wave length of FGM c: migration speed based of FGM

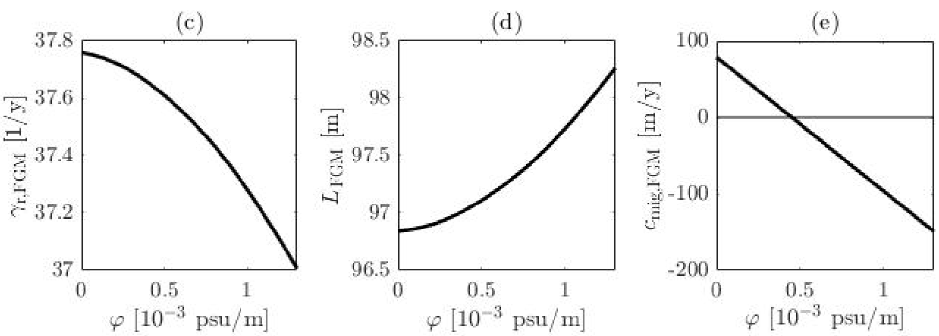

Figure 10: Sensitivity of the FGM to changes in the salinity gradient parameter range 0-1.3 (psu/km), a: Growth rate of FGM b:wave length of FGM c: migration speed of FGM

4.5. Salinity gradient

The salinity gradient in the sensitivity analysis ranges between 0 and 1.3 psu/km. Figure 10 presents the sensitivity to the salinity gradient . The salinity gradient has a relatively small impact on the growth rate of the FGM since this only ranges between 37 and 37.8. The growth rate decreases with an increase in a salinity gradient. A higher salinity gradient effect has some positive influence on the wavelength of the FGM. The salinity gradient has a negative linear effect on the migration rate of the sand dune. The salinity gradient can create a negative migration (upstream). Due to the river discharge, we have first a positive migration rate with a small salinity gradient. The modelled effect of the upstream migration is described in the literature and one of the reasons to include the gravitation circulation by van der Sande et al. (2021a).

4.6. Drag coefficient

The effect of vertical eddy viscosity is recalculated based on the range of the drag coefficient, which ranges between 0.0008 and 0.02 . Then the eddy viscosity varies between 0.016 and 0.4 m ^{2}/s. So the lowest implemented value for the drag coefficient leads to a smaller minimum eddy viscosity than the minimum eddy viscosity from the literature. Also for this lowest drag coefficient, the model is unable to present an accurately modelled perturbed flow. Figure 11 describes the sensitivity of the drag coefficient and indirectly the vertical

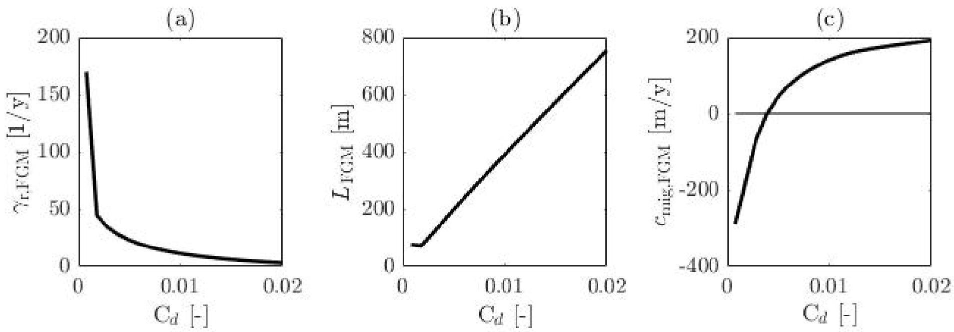

Figure 11: Sensitivity drag coefficient parameter range 8*10^{-4}- 2*10^{-2} (-), a: Growth rate of FGM b: wavelength of FGM c: migration speed of FGM. Point c_d= 0.008 has an inaccurately calculated perturbed flow and therefore presents an inaccurate calculation of this FGM

eddy viscosity. Lower values of the drag coefficient result in a high growth rate. With a slight increase in drag coefficient, the growth rate decreases fast. The wavelength of the FGM increases with higher drag coefficient values. With a small drag coefficient, the dunes migrate upstream. The migration rate decreases rapidly to zero when the drag coefficient increases. The larger drag coefficient values have a minimum impact on the migration rate. But still, the high drag coefficients have a maximum positive migration rate of 2*10^2 m/year downstream.

Next to the general increase and decrease of the output parameters of the FGM, the graph shows some strange behaviour with the smallest values of the drag coefficient. This unusual behaviour is a fast decrease in growth rate and a slight decrease in wavelength. This decrease is based on the calculation of the smallest drag coefficient, which results in inaccurate calculated perturbed flow.

4.7. Slip Parameter

The sensitivity of the slip parameter ranges from 0.0008 to 0.47 m/s and is presented in Figure 12. The growth rate increases with an increasing slip parameter. The slip parameter affects the shear stress at the bottom, and therefore the amount of sediment transport increases for a higher slip parameter based on the sediment transport equation. The slope between the growth rate and slipe parameter decreases with higher slip parameters. For small slip parameters, we find large wavelengths for the FGM. This wavelength rapidly decreases for higher slip parameters to wavelengths of the FGM between 50 and 200 meters. The slip parameter increases the migration rate with increasing slip parameters, based on a larger amount of sediment transport. However, it can not influence the direction of the migration of sand dunes.

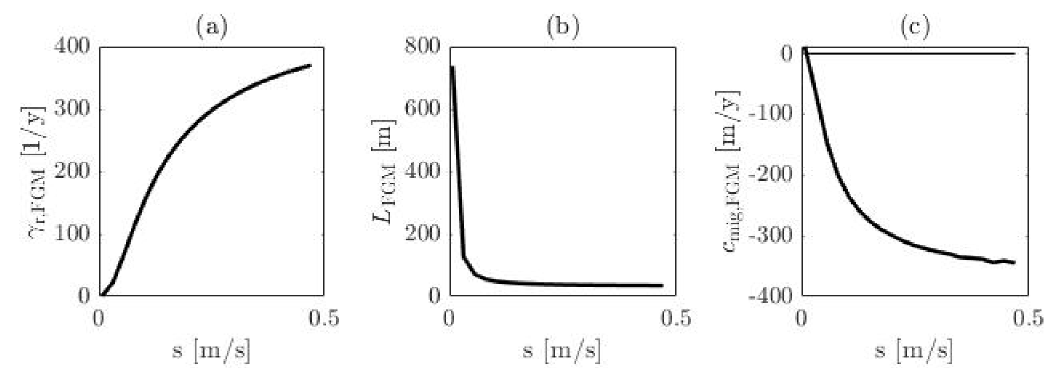

Figure 12: Sensitivity slip parameter range 0.007-0.47 (m/s), a: Growth rate of FGM b: wavelength of FGM c: migration speed based of FGM

4.8. Bed load exponent

Figure 13 shows the sensitivity to the bed load exponent, where the bed load exponent ranges between 1 and 3. This range in bed load exponent could also change other parameters within the model, however, in this case, only the bed load exponent is adjusted and not alpha (a scaling factor within the sediment transport equation). The growth rate of the FGM increases with an increasing bed load exponent. The bed load exponent has an enormous impact on the growth rate and migration rates since both have maximum values in the order of 10^3. Both increase exponential, and this could be expected since the bed load exponent is an exponent in the sediment transport equation and therefore increases rapidly the amount of sediment transport. However, the impact on the wave length is relatively smaller but still significant. The wavelength decreases with an increasing bed

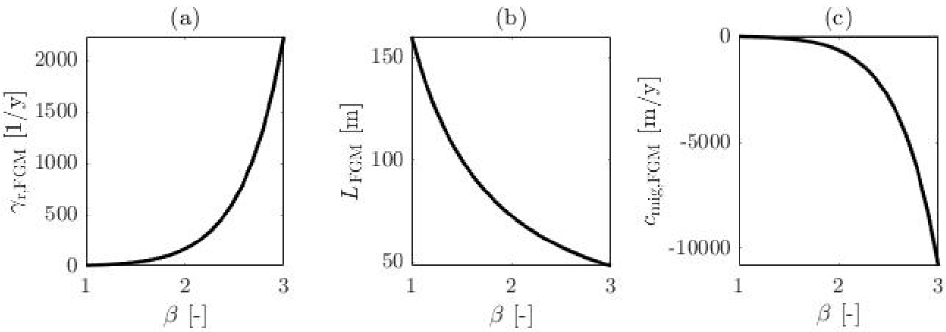

Figure 13: Sensitivity of the bed load exponent range 0.1-3.0 , a: Growth rate of FGM b:wave length of FGM c: migration speed based of FGM, the effect of the bed load exponent on the bed load coefficient is excluded.

load exponent. The largest values of bed load exponent give very large values of growth rate and migration rate that it is clear that this model parameter then overestimates the amount of sediment transport and therefore the growth and migration rates.

4.9. Slope correction factor

The slope gradient varies from 0.1 to 3. But, the model gives warnings for calculating the smallest slope corrections, since the model calculates a wave number larger than the range of wave numbers calculated. The results for a small slope correction seems to follow the

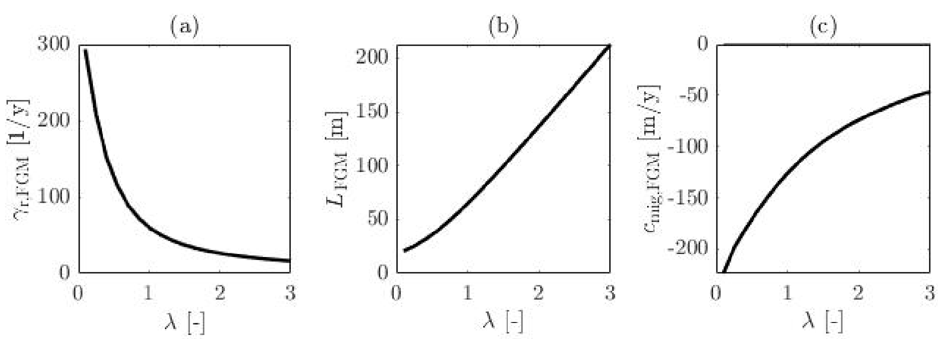

Figure 14: Sensitivity slope gradient range 0.1-3.0, a: Growth rate of FGM b:wave length of FGM c: migration speed based of FGM

pattern of the growth rate and migration rate. The migration rates for small values of the slope correction factor has a increase in migration for increases of the slope correction factor, while the rest of the graph decreases. Therefore this part of the migration rate is inaccurately represented by the wave numbers. The range of the wave numbers represents a range for sand dunes and smaller bed forms. The minimum of a slope correction of 0.1 is used in a model of river dunes wavelength of 0.6 meters Paarlberg et al. (2006) and this slope correction factor is found for a modelled river dune and these have a typical wave length which is smaller than estuarine sand dunes. Also, higher slope correction results in smaller values of sediment transport and therefore the growth rate is reduced. These higher migration rates for those smaller wavelengths is also expected since smaller bed forms can migrate easier.

4.10. Conclusion

This chapter shows that different parameters have a different local impact on the growth rate, wavelength and migration rate of the FGM. The bed load exponent, water depth and slip parameter have a large effect on the growth rate of the FGM. The salinity gradient, river current and tidal current have a minor impact on the growth rate of the FGM. Table 5 presents a summery of the effect of the different input parameters on the growth rate, wave length and migration rate. Please not that for the migration rate some of the parameters are able to change the direction of the migration (these are the water depth, depth-averaged M2 velocity amplitude, river discharge, salinity gradient and drag coefficient). While the other parameters only changes the amount of migration.

Table 5: The amount of impact of the parameter and the effect based on increases values of the parameter on the different FGM properties

	Growth rate (1/year)	**Wave length (m)**	**Migration rate (m/year)**
Water depth H (m)	Very strong decrease	Medium increase	Medium decrease
Depth-averaged M2 velocity amplitude U_{M2} (m/s)	Medium to small increase	Medium increase	Small increase
Depth averaged river flow velocity U_{res} (m/s)	Small increase	Very small decrease	Very strong increase
Sediment size D_{50} (mμ)	Small decrease	none	Very small decrease
Salinity gradient ϕ (psu/m)	Very small decrease	Very small increase	Very small decrease
Drag coefficient C_d (-)	Medium decrease	Strong increase	Medium increase
Slip parameter s (m/s)	Strong increase	Strong decrease	Medium decrease
Bed load exponent β_b (-)	Very strong increase	Medium decrease	Very strong increase
Slope correction gradient λ (-)	Strong decrease	Medium increase	Very small decreases

5. Effect environmental parameters compaired with the effect of empirical model parameters

This chapter describes the variations within the empirical model based on the environmental and empirical model parameters. The model uses ten different values for each parameter. Since we have 5 different environmental parameters, we have a large number of input variations than for the empirical model parameters. In the end, we look at the spreading of the fastest growing mode, its wavelength, growth rate and migration rate. Secondly, we look in this chapter at the combined effect of two parameters on predicted FGM properties. Herein we combine the parameters of the depth-averaged M2 velocity amplitude and the river discharge. The combined effect of the slip parameter and drag coefficient. Lastly, the combined effect of the bed load exponent and the slope correction factor.
The parameter ranges are changed based on the results of Chapter 4, so all inaccurate calculated parameter values are excluded from this analysis since this gives a false representation of the number of accurately calculated values. Also the range of the bed load exponent, β_b is limited, since the large values of beta overestimate the volume of sediment transport and therefore gives unrealistic values. The range of bed load exponent is changed to 1-2 as Campmans et al. (2017) suggested.

5.1. Environmental parameter dependency

In total 100,000 combinations of 5 different input parameters are used to calculate the FGM properties. However, only 66300 combinations of these model settings have an accuracy error of less than 10^{-4}, these parameter settings are used to describe the effect of the parameter changes on the FGM properties. Of the 66300 accurate calculations, 20 have a negative largest growth rate and therefore we expect no sand dunes by those driving forces and therefore we find no growth rate, migration rate and wave length. We also exclude the results where the sand dune wavelength is too small. Those small wavelengths are not sand dunes and they are not relevant for this research. Only 43460 of the total of 66300 accurate calculated have a wave number of less than 0.17 (so a sand dune wave length of at least 37 meters). Table 6 and Figure 15 present the spreading of the FGM data by changes in environmental parameters.

Table 6: Overview of the environmental parameter effects

	Growth rate (1/y)	Wave number ()	Wave length (m)	Migration rate (m/y)
Average	$2.34*10^2$	$8.51*10^{-2}$	$1.00*10^2$	$4.94*10^3$
Median	$9.49*10^1$	$6.91*10^{-2}$	$9.09*10^2$	$2.98*10^3$
Standard deviation	$4.50*10^2$	$4.75*10^{-2}$	$5.38*10^1$	$6.56*10^3$
Minimum	$2.10*10^{-1}$	$2.54*10^{-2}$	$3.15*10^1$	$-3.29*10^2$
Maximum	$4.62*10^3$	$1.99*10^{-1}$	$2.48*10^2$	$8.03*10^4$

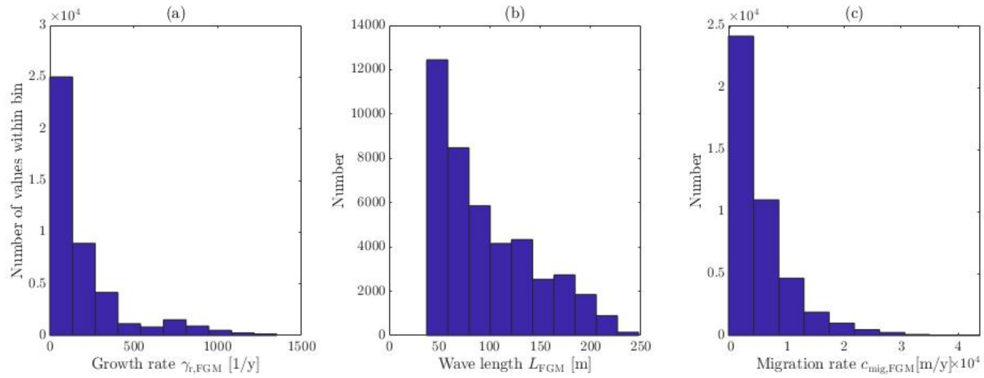

Figure 15: The environmental parameter dependency variation based on the a: the growth rate, b: wave length, c: migration rate.

5.2. Empirical model parameter dependency

The empirical model dependency uses 4 parameters so a total of 10,000 combinations of input parameters are used to calculate the FGM. The input parameters are the drag coefficient, slip parameter, bed load exponent and slope correction factor. 9000 combinations were calculated accurately with an error of 10^{-4} for the numerical solving of the perturbed state. Of the 9000 accurate calculated parameter sets only 6191 outcomes are within the limit of sand dunes wave lengths, 902 combinations give only negative growth rates. Table

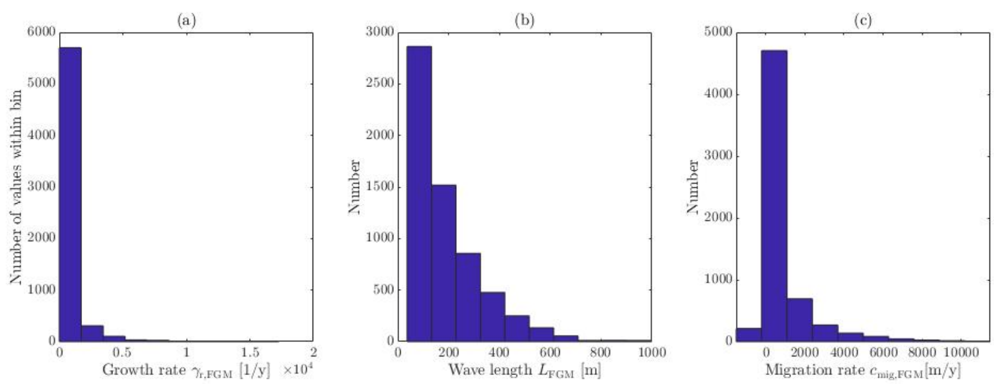

Figure 16: The empirical model parameter dependency variation based on the a: the growth rate, b: wave length, c: migration rate.

7 and Figure 16 present the spreading of the FGM data by changes in empirical model parameters.

Table 7: Overview of the empirical model parameter effects

	Growth rate (1/y)	Wave number (-)	Wave length (m)	Migration rate (m/y)
Average	$5.41*10^{2}$	$5.73*10^{-2}$	$1.87*10^{2}$	$7.63*10^{2}$
Median	$1.30*10^{2}$	$4.33*10^{-2}$	$1.45*10^{2}$	$2.22*10^{2}$
Standard deviation	$1.15*10^{3}$	$4.13*10^{-2}$	$1.43*10^{2}$	$1.41*10^{3}$
Minimum	$4.14*10^{-2}$	$6.29*10^{-3}$	$3.70*10^{1}$	$-1.52*10^{3}$
Maximum	$1.73*10^{4}$	$1.70*10^{-1}$	$9.98*10^{2}$	$1.15*10^{4}$

5.3. Difference environmental and empirical model parameter dependency

Since there are 5 environmental parameters and only 4 empirical model parameters, we see a difference within the number of model calculations, but also in the reductions based on accuracy and the wave length limitations. The environmental parameters have a higher reduction (34%) when the inaccurate calculated perturbed state is removed than the empirical model parameters (10%). The difference in the amount of reduction could be due to different reasons. One reason is that the number of parameters within the sensitivity analysis affects the number of inaccurate calculated model results. This inaccuracy is based on the solving of the calculation of the perturbed flow. For four of the five environmental parameters have an impact on the perturbed flow, while only the grain size is part of the sediment transport equation. While for the empirical model parameters, only two parameters have an impact on the perturbed flow (slip parameter and drag coefficient). The bed load exponent, β_b and the slope correction factor λ mainly impact the sediment transport equation.

The number of calculations with negative growth rates is significantly higher for the empirical model parameter sets (902), compared to the environmental parameter sets (20), while there are fewer parameter sets for the empirical model parameters. The empirical model parameters, including the slip, parameter have a larger impact on the calculated shear stress. This shear stress influenced sediment transport. If there is no significant shear stress, the sediment will not be transported, therefore the empirical model parameters have more influence on the sediment transport than the environmental parameters. Therefore the empirical model parameters have a larger number of results with negative growth rates. However the water flow within the water column is more affected by the tidal and river currents, but the eddy viscosity and the slip parameter influence more the effect around the bed and therefore the sediment transport. The reduction based on the limitation of a sand dune of at least 37 meters is for both cases (34% for environmental parameters and 32% for empirical model parameters) almost the same when including the reduction because of negative growth rates. However, when excluding the negative growth rates the reduction for the empirical model parameters based on wave length is reduced to 23%.

Figure 15 represents the variation of the FGM properties based on the accurately calculated sand dunes for the environmental parameter variation. Figure 16 represent the FGM variation of the empirical model parameter sets. The average growth rate of the environmental parameter is lower and the standard deviation of the growth rate is smaller In both cases, the average value is relatively closer to the minimum than the maximum value of the growth rate (so the average is higher than the median value). The average value and the standard deviation of the wave length are lower for the environmental parameter set compared with the empirical model parameter set. In both cases, the minimum wave length starts at 37 meters and the most calculated wave lengths are in the histogram bin closest to the value of 37 meters. This are the bins of between 37-109 meters for the empirical model parameters or between 37-58 meters for the environmental parameters. The number of results with larger wavelengths decreases with the wave length. The variation of migration rate is mainly dependent on the environmental parameters since this standard deviation is larger and the average value is also higher for the environmental parameters. The migration is mainly effected by the different forces of the migration (so the salinity gradient and river discharge), however the sediment transport equation has also a significant influence on the migration rates.

5.4. Effect of two parameters

Now we compare the effect of two environmental or two empirical model parameters on the FGM properties. For the empirical model parameters, we compare the effect of the depth-averaged tidal velocity amplitude and the depth-averaged river flow velocity. For the empirical model parameters, we combine the effect of the slip and drag coefficient and secondly the effect of the bed load exponent and the slope correction factor.

5.4.1. Depth averaged M2 velocity amplitude and the river discharge

Those parameters are both environmental parameters and both affect the flow velocity within the water column and together they form a balance between the tide and the river discharge. The river discharge is a one-directional flow, however, the tidal flow implemented is symmetrical.

Figure 17 describe the combined effect of the velocities of the tidal current and river flow. This figure shows that the model currently is unable to calculate the results accurately for low values of the depth-averaged tidal velocity amplitude especially combined with higher values for the depth-averaged river flow velocity. This inaccuracy is also visible in the figures by the large variations between one cell and the next cell within the wave number graph and the migration growth rate graph. The wave number graph shows that the depth-averaged tidal velocity amplitude has the largest influence on the wave number, for larger values we find a smaller wave number and therefore larger wave lengths. The growth rate is also mainly influenced by the depth-averaged tidal velocity amplitude and larger values decrease the growth. The migration rate is influenced by both, the depth-averaged river flow velocity and depth-averaged tidal velocity amplitude. With lower values, the migration decrease and is even negative for the smallest values of both parameters combined due to the effect of the salinity gradient. Based on the analysis of Chapter 4 these results could be predicted, except that the tide has also a significant influence on the amount of migration when those parameters are combined. The graph of the migration rate shows mainly that those parameters interact with each other.

5.4.2. Slip parameter and drag coefficient

The slip parameter and the drag coefficient are two empirical model parameters, that affect the boundary conditions on the bed. The slip mainly acts on the water flow at the bottom and the drag coefficient influences the modelled water flow in the water column and less on the bed. Figure 18 show that for the smallest values of the slip parameter, we find no positive growth rate, therefore these locations are white in the graph. Also, the values for the smallest drag coefficient are inaccurately calculated, this shows in some big changes in this line between neighbouring cells. The drag coefficient has more impact on the wave number than the slip parameter, however, the wave number decreases a little for higher slip parameter values. The slip parameter mainly influences the variation of the growth rate, larger values increase the growth rate due to more slip at the bed, however, the increase in drag coefficient decreases the growth rate. The drag coefficient has a larger impact on the calculated migration rates compared to the slip parameter, while Chapter 4 describes that they have almost the same influence on migration. The lower values of the slip parameter still decrease the migration, however mainly the larger values of the drag coefficient increase the migration rate, due to more turbulence within the water column since there is a higher eddy viscosity.

5.4.3. Bed load exponent and the slope correction factor

The bed load exponent and the slope correction factor are two empirical model parameters, part of the sediment transport equation. The bed load exponent increases the volume of sediment transport and therefore the growth rate and migration rate. However, the slope correction factor decreases the predicted volume of sediment transport and therefore the predicted growth of the sand dunes and their migration. This combined effect is represented in Figure 19. The slope correction factor has a larger influence on the wave number than the bed load exponent, however, the higher values of the bed load exponent increase the wave number a little. In the calculation, the slope correction factor affect the larger wave numbers (so smaller wave lengths) more since the smaller wave lengths have with the same bed amplitude a steeper slope and therefore more correction than larger wave lengths. This is comparable with a small slope correction for a river dune Paarlberg et al. (2006). Both the slope correction factor and the bed load exponent have a large impact on the growth rate. The large values of the slope correction rate values reduce the growth rate, while the increase of the bed load exponent increases the growth rate. The top left values have smaller growth rates, while the bottom right has a larger growth rate. Almost the same pattern is seen for the migration rate, less migration in the parts with smaller growth rates and the largest migration for a small slope correction factor and a large bed load exponent.

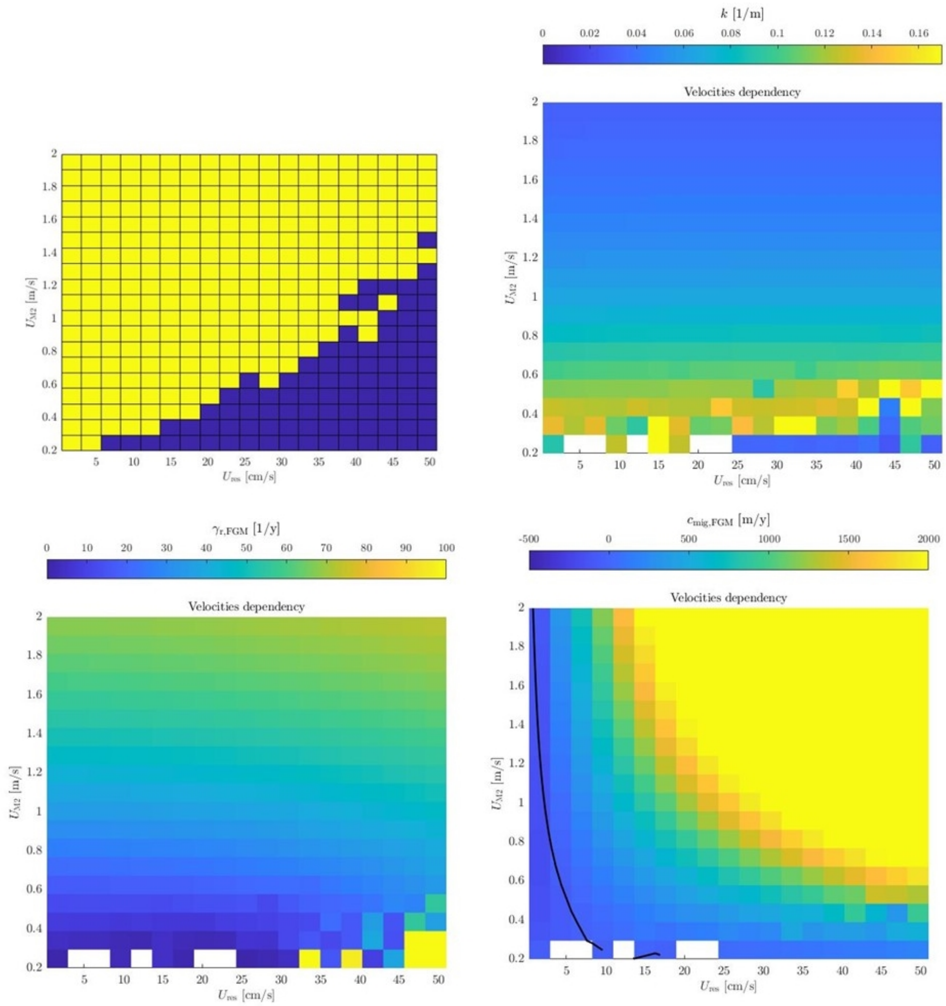

Figure 17: The combined effect of the depth averaged river flow velocity on the x-axis and the depth averaged tidal velocity amplitude on the y-axis and their effect on FGM. The top left figure represents the accuracy of the calculation, with blue inaccurate. Top right the wave number, bottom left growth rate and bottom right migration rate.

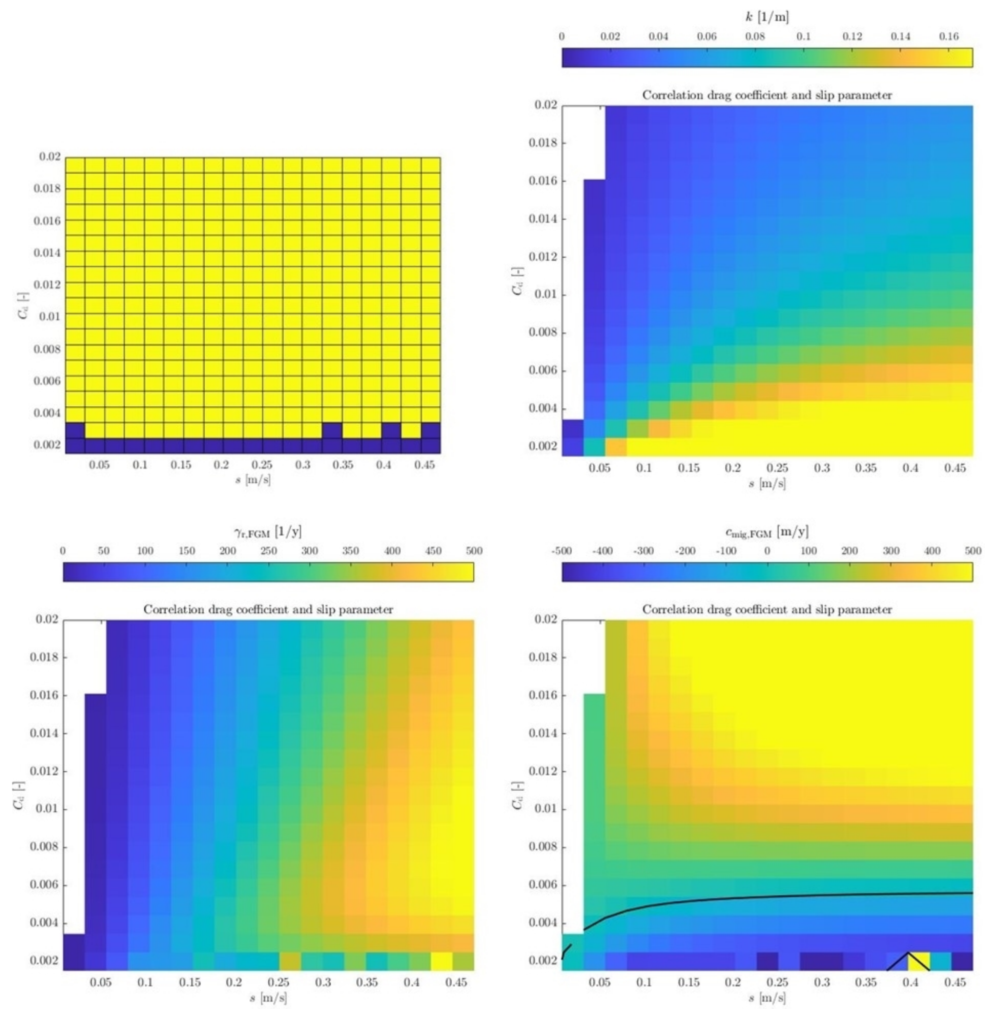

Figure 18: The combined effect of the slip parameter on the x-axis and the drag coefficient on the y-axis and their effect on FGM. The top left figure represents the accuracy of the calculation, with blue inaccurate.Top right the wave number, bottom left growth rate and bottom right migration rate.

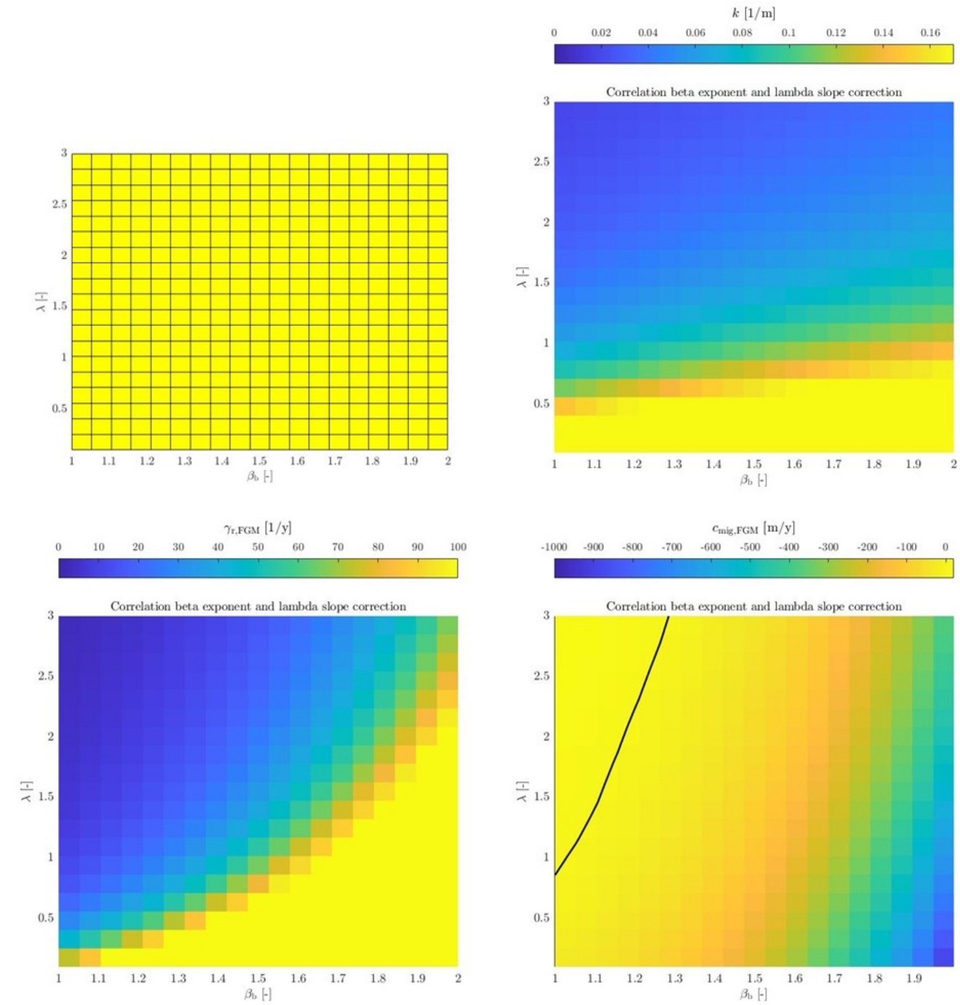

Figure 19: The combined effect of the bed load exponent β_b on the x-axis and slope correction factor λ on the y-axis and their effect on FGM. The top left figure represents the accuracy of the calculation, with yellow all accurate calculated perturbed flows. Top right the wave number, bottom left the growth rate and bottom right migration rate.

6. Validation of the model

This chapter describes the validation of the current model of van der Sande et al. (2021a). First, we present the validation locations by their environmental parameters, combined with the values of the Gironde estuary. Second, the results of the adjustment of the environmental parameters are presented. The third step describes the amount of adjustment in the slip parameter for a re-calibration.

6.1. Environmental parameters

For the validation of the sand dune model of van der Sande et al. (2021a) we look at three new locations in two estuaries, the Scheldt estuary (locations Vlissingen and Terneuzen) and the Elbe Estuary (sand dunes near Grauerort) Table 1 presents an overview of several sand dunes at these estuaries, however, for the validation, we only use the selected locations. Table 8 represents the sand dunes located at the sites named above. The sand dunes at Grauerort have relatively small wave lengths between 20 and 38 meters. In Chapter 5 they were classified as smaller bed forms and there excluded but, in this chapter, these sand dunes are included.

Table 8: Sand dunes located at the locations of the model validation

Estuary	**Location**	**Wave length [m]**	**Wave heigth [m]**	**Depth [m]**	**Migration**	**Source**
Elbe	Grauerort	20-38 mean 30	1.3-2.2 mean 1.7	20		Muurman (2021)
Gironde	Royan	37-182 mean 84	1.5-6.7 mean 4.9	20-30	Downstream crest migration	Schrottke et al. (2006)
Western Scheldt	Vlissingen	155-330 mean210	1.7-3.4 mean 2.6	20-25		Muurman (2021)
Western Scheldt	Terneuze	30-120 mean 65	0.6-2 mean 1.25	35 max		Muurman (2021)

Table 9 describes that there are variations in all 5 environmental parameters. Some of the variations in the parameters have smaller effects than others, especially the combination between the difference within the depth-averaged tidal velocity amplitude and the depth-averaged river flow velocity can have significant changes and therefore some impact.

Table 9: The environmental parameters for different locations and estuaries, [a] Muurman (2021) [b] Vandenbruwaene et al. (2013) [c] Chapter 3 and Appendix A [d] van der Sande et al. (2021a)

Parameter	**Unit**	**Gironde**	**Scheldt estuary (Vlissingen)**	**Scheldt estuary (Terneuze)**	**Elbe estuary**
Mean water depth (H)	m/s	20	22 [a]	25 [a]	20 [a]
Depth averaged tidal amplitude (U_{M2})	m/s	1	1.3 [a]	1.05 [a]	0.7 [a,b]
Depth averaged river flow velocity (U_{res})	m/s	0.0031-0.022 [c]	0.0040-0.0071 [c]	0.0045-0.0079 [c]	0.01-0.06 [c]
Grain size(d50)	μm	350	289 [a]	299 [a]	407
Longitudinal salinity gradient (ϕ)	psu/m	0.6 [d]	0.4 [b]	0.4 [b]	0.38 [b]

6.2. Validation for three other locations

The validation of the three locations is done based on the different input parameters and the results of the FGM properties. We compare this data with data of the sand dune sizes described earlier in Table 1. Herein is especially the wave length the most relevant. The model output is shown based on a variation in the depth-averaged river flow velocity on the x-axis since there is some variation within this parameter and therefore the total range is presented. The range in wave number differs between the estuaries since the range partly describes the accuracy and also depends on the expected sand dunes wave lengths based on the data in Table 8.

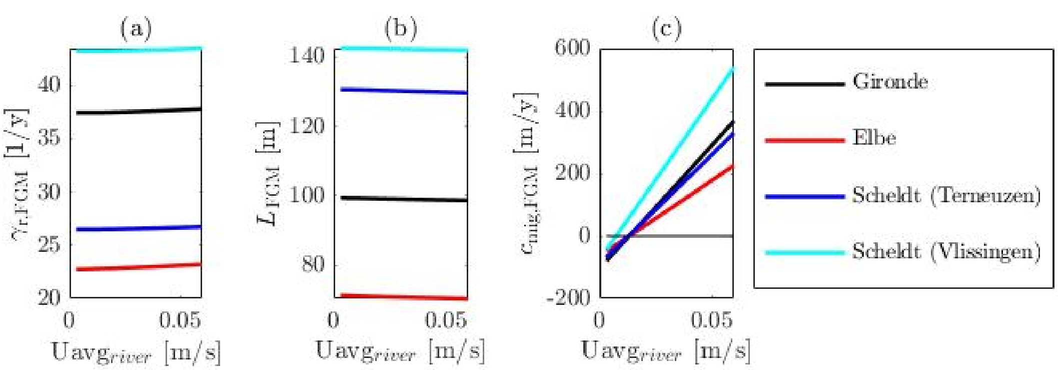

Figure 20: The validation of the model based on 4 different sets of input parameters, of which the Gironde is the calibrated set and the other 3 locations are for validation

This current model is calibrated based on the environmental parameters and the outcome of the Gironde Estuary. However, the model is calibrated by adjusting the value of the slip parameter based on the wave lengths of the sand dunes in the Gironde estuary, therefore the modelled FGM wave length varies a little bit more, however, Figure 20 presents that the FGM calculated wave length of the Elbe is the smaller compared with the wave length of the Gironde and the Scheldt Estuary. However, the wave length at the Scheldt at Terneuzen is overestimated and even higher than the Gironde, while in reality, the values of the wave length of the sand dunes Scheldt at Terneuzen are in the same order or slightly smaller than the values of the sand dunes of Gironde estuary. So, the model underestimates the differences between the modelled FGM wave length and the wave lengths found in case studies. For example, the wave length predicted for the Elbe estuary at Grauerort is 71 meters, however, the range in wave lengths measured is between 20-38 so even less than half of the wave length predicted. Also, the wave lengths at Vlissingen are underestimated in the model ($1.3*10^2$) while the site study shows larger sand dunes (155-330 meters with a mean of 210 meters). So the model can predict how the sand dunes wave length differs between locations, however the model under and overestimates the wave lengths.

The migration rates of the Gironde and the two locations of the scheldt combined with the smaller values in river discharge on these locations present a negative migration rate. So the model predicts an upstream migration of the sand dunes. For the Elbe estuary the migration depending on the discharge can be both positive (max of 200m/year) and negative (minimum of -16 m/year). The maximum of 200m/year compared with measurements of estuarine sand dunes migration is relatively high, however is still reasonable for this model. This research did not find dune migration data at the location of Grauerort, however the dune migration rates corresponds with the data of sand dunes closer to Hamburg. The direction of the migration, in the model and measurement for the Scheldt at Vlissingen is negative and relatively small. The direction of the dune migration is in the same , so the migration rate is more correct at this location than the wave length. For the Gironde, the model predicts a landward migration for the current values and for large river discharges this migration direction switch to seaward migration. Since the measurement show small river discharges the model calculated a negative migration, but based on the paper of Berne et al. (1993) we would expect a positive seaward migration. The model calculated a negative migration at Terneuzen (Western Scheldt) there are no measurements of sand dune migration here, but since we found both landward (downstream of Terneuzen) as seaward (upstream of Terneuzen) migration we can not say anything about this direction of this computed migration.

So the values of the migration rates of the sand dunes are in the correct order of magnitude, however we do not always have measurements to compare this data. However the direction of the migration is only incorrect for the Gironde estuary, and for the Terneuzen location the direction of the migration can not be determined based on the local measurements. So the current values of the slip parameter give a relatively good image of the amount of migration, however the calculated wave lengths are under and overestimated for the current value of the slip parameter.

6.3. Calibration for other location

Since the model over and underestimates the wave lengths for other locations than the Gironde Estuary, the slip parameter is re-calibrated for these other estuaries. The migration rates may not increase since the current model already overestimates the migration. The amount of changes in the slip parameter is an indicator for future use of the model and the amount of re-calibration needed. The current slip parameter in the model is 0.04 ms^{-1}

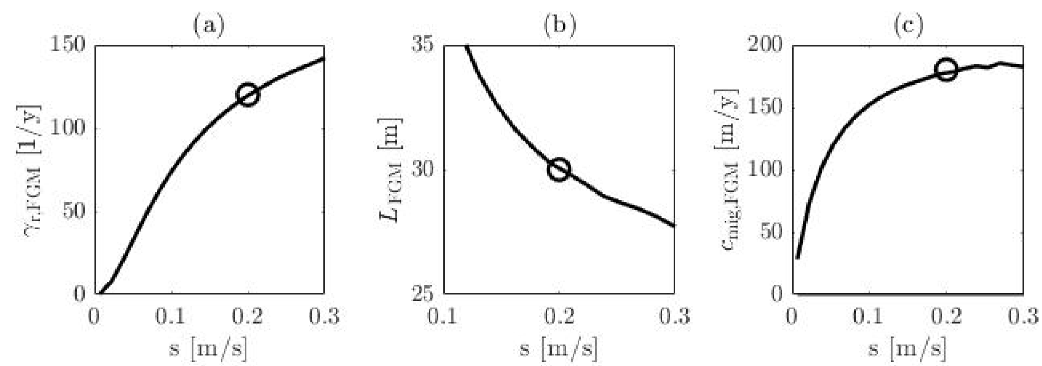

Figure 21: The calibration of the slip parameter for the Elbe estuary at Grauerort. a) The corresponding growth rate, b) The wave length limited around the mean wave length c) the corresponding migration rate

The calibration graph in figure 21 shows that a slip parameter of 0.2 ms^{-1} is needed to find a wave length of 30 meters for the local environmental parameters of the Elbe estuary. In this graph not all parameters are calculated accurately, however, the values around the point s= 0.2^{-1} are calculated accurately. For this value, we find a growth rate of 1.2 *10^2/year, a wave length of 30 meters (k=0.21 /m) and a migration rate of 1.8*10^2 m/year (was 1.010^2 meter/year for s= 0.04 ms^{-1}). However also the amount of migration increases by the increase of slip parameters and therefor the migration rate increases in the model. Since we find a migration rate of 55 meters/year for the larger sand dunes (L=46 meters) located at Hamburg, the value of 1.8*10^2 m/year is relatively large however could be reasonable for those smaller dunes. So the slip parameter of 0.2 ms^{-1}, 5 times larger than for the Gironde estuary case gives a more correct wavelength however also increases the migration rate .

The calibrated slip parameter of the Scheldt estuary at Vlissingen is 0.028 ms^{-1} to find a wave length of 210 meters. Figure 22 shows the calibration. For this value, we find a

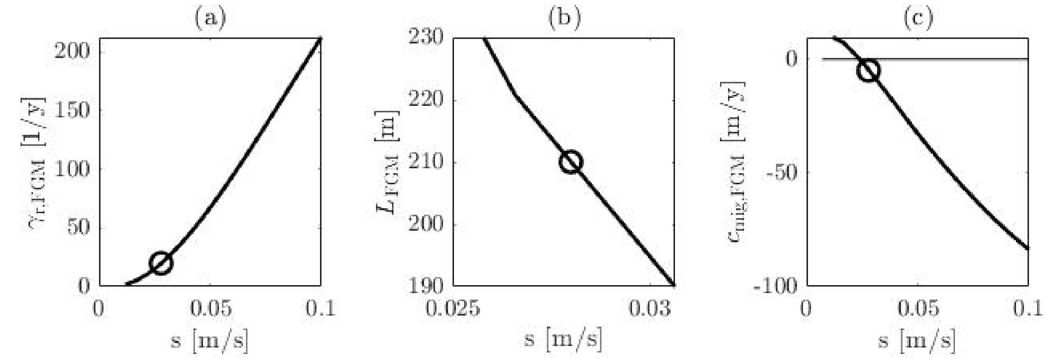

Figure 22: The calibration of the slip parameter for the Scheldt estuary at Vlissingen. a) The corresponding growth rate, b) The wave length limited around the mean wave length c) the corresponding migration rate

growth rate of 20/year (was 40/year), a wave length of 2.1*10^2 meters (k=0.030/m) and a migration rate of 5 meters/year (was 20 meters/year). The values of the growth rate and migration rate of the dunes decreases due to a smaller slip parameter, but both values before and after the calibration could be realistic for these sand dunes. The calibrated slip parameter is almost half of the slip parameter of the Gironde estuary case.

The Gironde model overestimates the wave length of Scheldt estuary at Terneuzen. The re-calibration of the slip parameter gives a new slip parameter of 0.088 ms^{-1} to find a wave length of 65 meters. Figure 23 shows the calibration. For this value, we find a growth rate of 95/year, (was 27/year) a wave length of 65 meters (k=0.097/m) and a migration rate of 1.2 *10^2 meter/year (was 50 meters/year). The slip parameter is more than twice the value of the slip parameter of the Gironde estuary case.

So the calibrated slip parameters range between 0.028 and 0.2 ms^{-1} based on the wave lengths. These values are within the ranges of the slip parameter earlier found in Chapter 3 and between half and five times the value of the Gironde. The larger values of the slip parameter also increases the migration and growth rates, so the maximum value of the slip parameter of 0.2 ms^{-1} is relatively large. The calibrated value is not constant for one estuary. And if the model needs to perform with one value for the Scheldt, the slip parameter of the Gironde is between the two calculated slip parameters for the Scheldt, however, the slip parameter depends on the location within an estuary and not on the estuary.

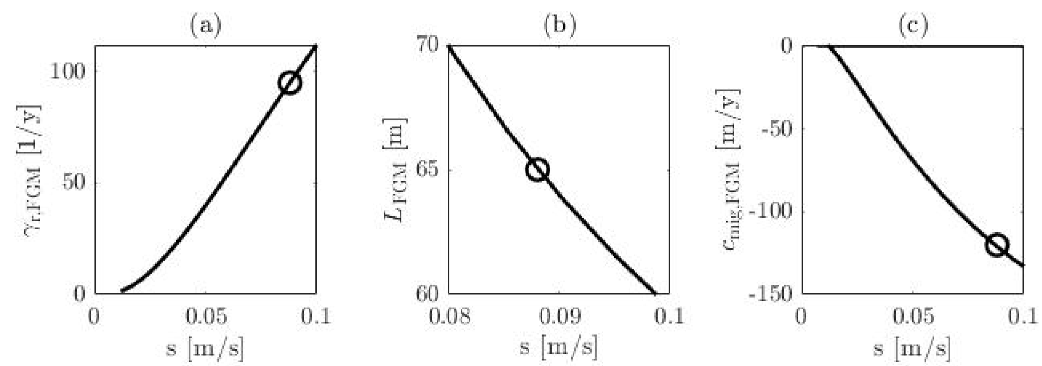

Figure 23: The calibration of the slip parameter for the Scheldt estuary at Terneuzen. a) The corresponding growth rate, b) The wave length limited around the mean wave length c) the corresponding migration rate

7. Discussion

This chapter discusses the conducted study. The first part of the discussion is about the methodology decisions, the second part discusses the results and

7.1. Methodology

In the methodology several decisions are made, however, they impact the methodology and therefore the research.

7.1.1. Selection of estuaries

In this study, the parameter ranges are based on a review of 5 selected estuaries. Four of these five estuaries are located in West Europe, therefore the parameters are more influenced by the same weather and insights inside discharge control and insights of the dredging of the bed. Those influences can limit the ranges in parameters. The outcome may be different using a different selection of estuaries and different sources for the estuary data. One of the challenges is the definition of an estuary. For example, the Bahia Blanca (Argentina) is by some definitions classified as an estuary, however, in this case, the discharges of the rivers are insignificant compared with the amount of the incoming tidal wave and therefore this study will classify it as a bay instead of an estuary. This difference in definition has some influence on the ranges in parameters.

7.1.2. Classification of sand dunes based on wave lengths

This study uses in Chapter 5 a minimum wave number of 0.17 however, the sand dunes described in Table 1 have wave lengths smaller than 37 meters (wave number of 0.17). The definition of a sand dune, therefore, varies within this study and also other studies differ about the definition and size of an estuarine sand dune. Similar to the definitions of marine sand waves and river dunes, they partly differ between studies. Although papers differ in definition, the paper of Ashley (1990) is widely cited for the classification of the sizes of sand waves in marine environments. The sizes of the sand dunes in an estuary depend on the location within the estuary. For example, the sand dunes sizes at the mouth of the estuary close to the sea or ocean are more influenced by the marine than fluvial processes and therefore the dimensions are closer to marine sand waves than the smaller river dunes.

7.1.3. Indirect influence of parameters

Currently, all input parameters are addressed as if all parameters are independent correlated of each other. However, there could be some discussion if all parameters change independently of each other. For example, the water depth is one input parameter, however, this parameter is closely related to the depth-averaged river flow velocity (calculated based on cross-section and river discharge) and possible the depth-averaged M2 velocity amplitude. Next, the parameters in the sediment transport equation affect each other. The parameters bed load exponent β_b, slope correction factor λ and the bed load coefficient α_b together are the empirical parameters which could be changed based on the fitting of the measured sediment transport and the calculated sediment. This bed load coefficient could therefore be a scaling factor and this scaling based on different bed load exponent or slope correction is not included in the current model. Also the sediment size is now only included by the recalculation of the bed load coefficient α_b, however the grain size has also some impact on other parameters. BAGNOLD (1956) describes that the slope correction factor depends on several factors, one of them is the sediment size, earlier was this effect excluded in the model. Also the sediment size influences the calculation of the drag coefficient, since this parameter is mostly calculated based on the balance of the drag force and the forces of the gravity (Arora et al., 2010). So both the environmental parameters and the empirical model parameters are correlated within the group of parameters however even the empirical parameters depend on the environmental parameters. So the effect of one single parameter change is underestimated in this model. Therefore the effect on the FGM properties could be over-or underestimated.

7.1.4. Incorrect calculation of the growth rate of the FGM

The large sand dune model consists of several subparts. The sub-model FGM_calc is responsible to calculate the FGM properties based on a vector of dimensional growth rates and migration rates for a vector of wave numbers. These vectors of the growth rates and migration rates are earlier in the model calculated. The model published van der Sande et al. (2021b) has only a few checks. The first check is that the maximum growth rate is positive (else there are no sand dunes) and if the corresponding wave length of the maximum growth rate is smaller than 1000 meters (these large wave lengths are not expected). The second check is whether the wave number belonging to a certain maximum growth rate is not the maximum wave number. If so, this leads to a warning, but the model calculations continue. Then a 3-dimensional polynomial curve fitting (polyfit) is made for the growth rate to calculate the maximum growth rate. Based on the derivative of this polyfit the location of the maximum growth rate is calculated. However for some parameter sets the growth rate has no local maximum based on the derivative (based on the ABC formula, Figure 24 is an example of a polyfit with no correct calculated maximum growth rate) and the location of the maximum (so the value of the wave number) includes an imaginary part. The growth rate calculated has also an imaginary part, however, the model is unable for calculating its migration rate at this location due to the imaginary sub solution of the model, and the model stops its calculation. The model is adjusted to use in this case the location of the maximum growth rate (at one of the calculated values of k) and not the maximum of the polyfit. Based on this maximum growth rate its corresponding migration rate is selected. and the model can calculate the other sets of input parameters.

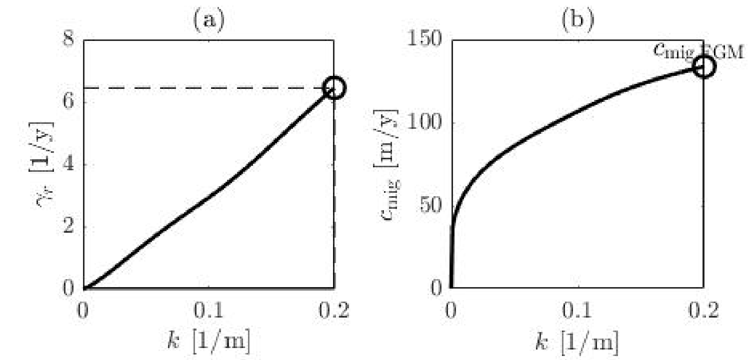

Figure 24: Example of a growth rate and migration curve where there is no maximum calculated growth rate. (H=10.83m,U_{M2}=0.2m/s, U_{res}=0.17m/s, ϕ= 1.16 psu/km, D_{50}=634μm

7.2. Results

The discussion also discusses the results of the research questions. This discussion consists of the effect of the limitation in wave length, the eddy viscosity formulation, the estimation of water depths and their effect on the validation.

7.2.1. Eddy viscosity formulation

The vertical eddy viscosity is calculated following Prandle (1985) approach ($A_v = c_d H U_{M2}$). Herein is c_d the drag coefficient, H the mean water depth and U_{M2} the depth-averaged tidal velocity amplitude. However, Figure 17 shows that the model has some problems in calculating the perturbed flow for low values of the depth-averaged M2 velocity amplitude combined with higher values of the depth-averaged river flow velocity. One of the reasons for these inaccurate results could be that the eddy viscosity now only depends on the tide, however, the inaccurate perturbed flow results present themselves when the river flow and the tide both have a significant influence. Three possible solutions are tested to change the velocity component in the eddy viscosity equation: 1) the maximum velocity of U_{M2} or U_{res} is implemented 2) the sum of both U_{M2} or U_{res} is the velocity component 3) Pythagoras is used to combining the two velocities. The first solution gives almost the same results in all four sub-graphs and has still a large part where the perturbed state is inaccurately calculated. The second solution is presented in Figure 25. For this solution, all combinations of values are calculated accurately. The third solution is presented in Figure 26. For this solution, only a few combinations of values are calculated inaccurately. Therefore solutions 2 and 3 could both work for an improvement of the eddy viscosity in the cases of a small depth-averaged tidal velocity amplitude. However solution 3 uses a smaller value of the U implemented for the calculation of the eddy viscosity, therefore the difference in the U for higher values of the depth-averaged tidal velocity amplitude is less and this solution is closer to the already implemented solution in the model as suggested by van der Sande et al. (2021a).

7.2.2. Estimation of the water depth in validation

For the validation of the model used in this study, an estimation is made of the water depth based on sources and a cross-section of the area with sand dunes. However this water depth should represent the average depth of the sand dune field and therefor one measurement on a bed with sand dunes, can overestimates the water depths at Vlissingen and Terneuzen in the Scheldt. When excluding the difference in the model based on the locally measured depths (Figure 27, the spreading of the wave length based on the other parameters, is closer to the measurements of the case studies at those locations. The wave length at the location of Terneuzen is now closer to the wave length at the Gironde estuary. In the case studies, the ranges of wave lengths of these two locations have a large overlap and the mean wave lengths measured at these sites vary less between those two than in the other locations. So the situation with all the same water depth better represent the spreading of the wave lengths between the different locations.

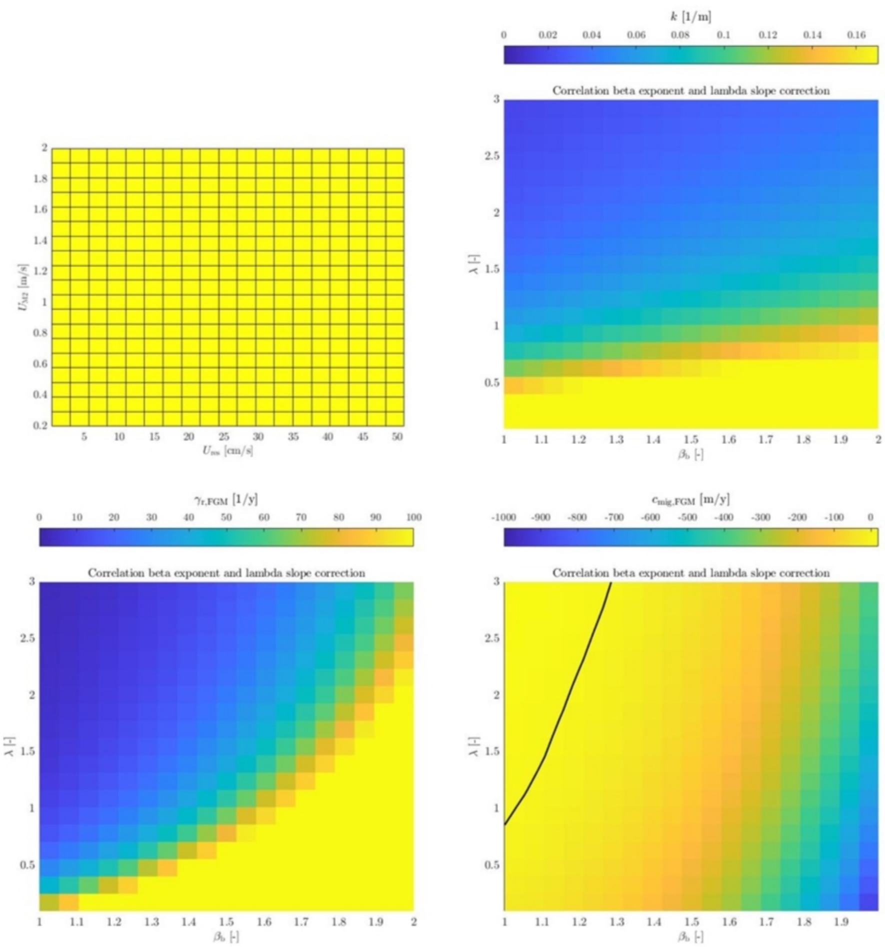

Figure 25: Solution 2 (sum of the velocities): The combined effect of the depth averaged river flow velocity on the x-axis and the depth-averaged tidal velocity amplitude on the y-axis and their effect on FGM. The top left figure represents the accuracy of the calculation, with blue inaccurate. Top right the wave number, bottom left growth rate and bottom right migration rate.

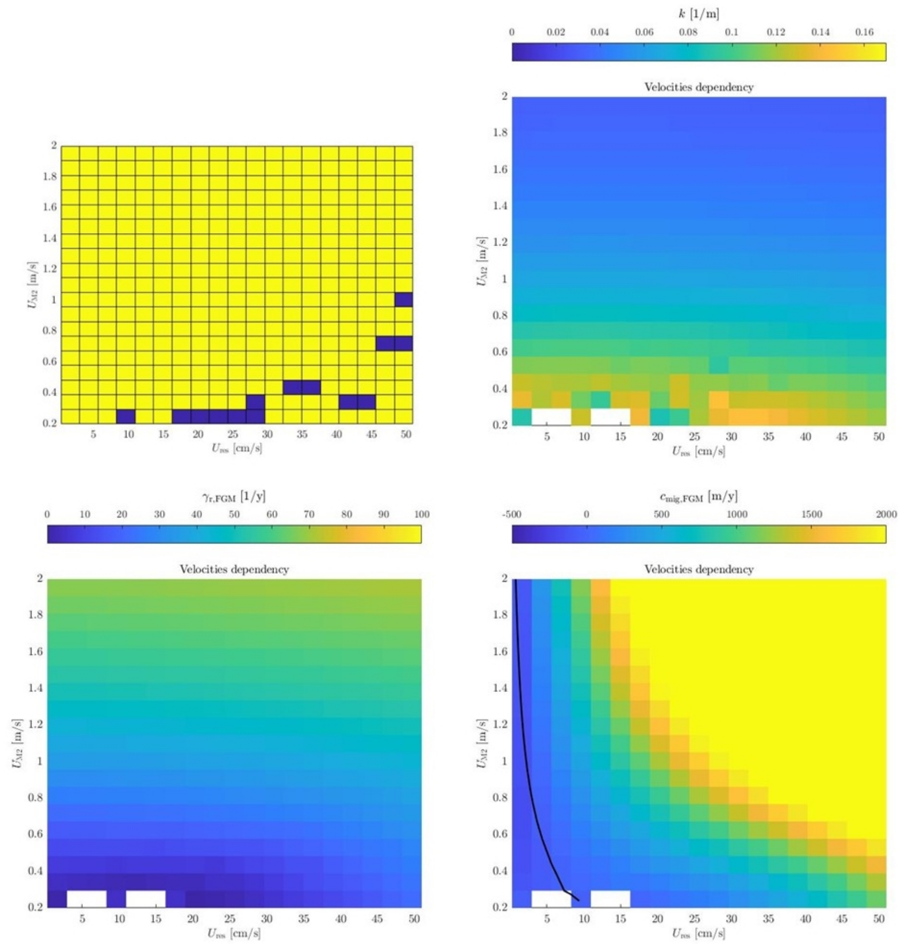

Figure 26: Solution 3 (Pythagoras with the velocities) :The combined effect of the depth-averaged river flow velocity on the x-axis and the depth-averaged tidal velocity amplitude on the y-axis and their effect on FGM. The top left figure represents the accuracy of the calculation, with blue inaccurate. Top right the wave number, bottom left growth rate and bottom-right migration rate.

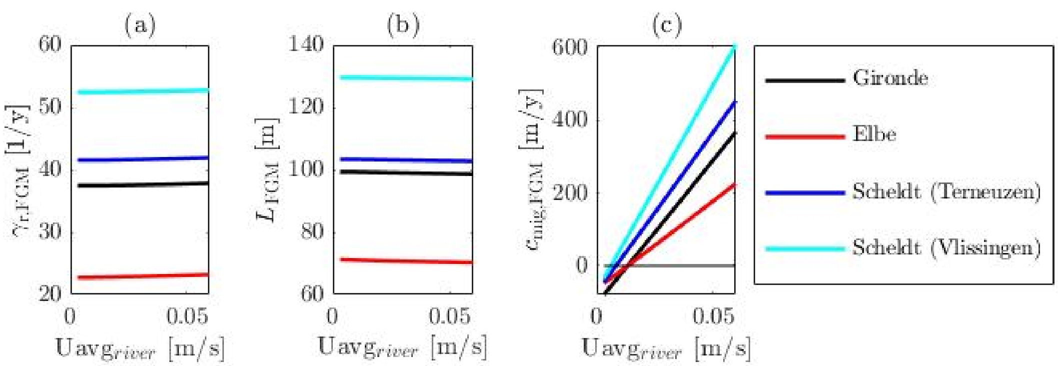

Figure 27: The validation of the model based on 4 different sets of input parameters with the same water depth of 20 meters, of which the Gironde Estuary is the calibrated set and the other 3 locations are for validation

8. Conclusion

This study evaluates whether the model of van der Sande et al. (2021b) can be used to learn about the formation of estuarine sand dunes and looks into the validation of the current model. There are two types of parameters used to understand the formation of sand dunes, the environmental parameters and the empirical model parameters. The environmental parameters are depending on the environment of the sand dunes in an estuary, those are the water depth, the depth-averaged M2 velocity amplitude, the depth-averaged river flow velocity, grain size and salinity gradient. The empirical model parameters are more indirect depending on the environment. The model parameters are the drag coefficient, slip parameter, bed load exponent and slope correction factor.

What are realistic values for model parameters used in the model for estuaries with sand dunes ? Chapter 3 describes the literature study preformed to find the ranges in the model parameters used for the following questions. Table 3 present the ranges in the parameters. Most of these parameters ranges are based on 5 estuaries, while others are based on suggestions and ranges of other researchers. Some of the ranges within one parameter seems larges, due to a order difference between the smallest and the largest value.

What are the effects of one individual parameter changes on the fastest growing mode ?
By implementing the estuarine parameter ranges (Chapter 3) into the model to study the effect of individual parameters, we see that the literature-based parameter ranges can cause some problems in the solving of the flow of the perturbed state. However, in most cases, only a small part of the parameter range has an inaccurate solution for the perturbed flow model. Therefore the results of the effects of one individual parameter change on the FGM properties can still be evaluated. Each of the nine parameters has a different effect (and amount of effect) on the FGM properties. For example, the mean sediment size has a relatively small influence on the growth rate, migration rate and the corresponding wave length, while for the slip parameter only the small values have a large influence on the wave length, while the larger values have a much smaller impact on the wave length. Table 5 gives an overview more in-depth overview of all parameters in Chapter 4

What is the combined effect of varying the environmental or empirical model parameters of question 2 on the fastest growing mode and its corresponding migration rate?
The environmental parameters combination have a larger impact than model parameters combinations on the migration rate. However, the model parameters have a larger range in the growth rates and wave lengths. In both cases, the results of the wave length of most parameter sets are close to the boundary of what a sand dune is. Also for the growth rates and migration rates graphs, there is one large bin in the histogram, with median lower than

the average values. This means that a large number of calculations have a relatively low value and a few extreme values increase the average.
The next step was to combine two input parameters change to affect the FGM properties since these interact with each other and therefore these combined changes are sometimes a little different than the individual changes in a parameter. Three combinations of parameters are implemented: 1) the tide and river discharge, 2) the slip parameter and drag coefficient 3) the bed load exponent and the slope correction factor. The analysis of these combinations shows that sometimes mainly one parameter determines the FGM properties (the tide for the combination tide and river combined except for the migration rate). While the other two combinations of parameters have more interaction between the two input parameters and therefore affect all three parameters of the FGM properties. Some of the results could be explained by the results of Chapter 4, however, these combinations give some new insight into sand dunes formation due to changes in both parameters.

How representative is the sand dune model of van der Sande et al. (2021a) with its current values for the Elbe and Scheldt estuary?
The model of van der Sande et al. (2021a) can be used to understand the formation of sand dunes. The current model is calibrated for one location and some of the effects changed by the environmental parameter can be explained by the current settings of the model. The slip parameter now resembles a value for the Gironde Estuary, but based on the analysis of Chapter 6 we have seen that a re-calibration of the slip parameters better represent the sand dunes wavelengths, however, the current model can still help in understanding the initial development of sand dunes without the re-calibration.

9. Recommendations

This current research is conducted based on the assumption that: 'the individual input parameters do not influence each other'. The discussion (Chapter 7) described that some of the parameters influence each other. The relations between the input parameter is not researched in this study, however, could be relevant for further use of the current model.

Secondly, Muurman (2021) describes the presents of an asymmetrical tide for the locations of the Western Scheldt estuary. The current calculations only are done with an M2 tide. However, the model can include the combination with an M4 wave or higher orders. This will affect the FGM properties and is currently not investigated. Those changes in input parameters help to better represent the local environmental values and help to better present the local environment in the model. It could help to better understand the differences in wave lengths between estuaries and therefore it could be relevant for further investigation.

The current study looked into the initial growth of the sand dunes based on linear stability analysis and individual parameters changes. However, the effect of a parameter changes when the sand dunes are well developed. Then the sand dunes affect the hydrodynamics of the system. In the validation are some of the differences between dynamics of the system and the expected wave lengths explained, however a more in-depth study of these cases can help to even better understand the differences between wave lengths of sand dunes in estuaries. Herefore a study with a full 3D model like Delft3D can help understand the currently missing link that explains the wave lengths between estuaries since the current model only gasps. However, this full 3D model approach is a more complex model. This method takes more time to evaluate one estuary.

Bibliography

Adey, W. H. and Loveland, K. (2007). Chapter 22 - estuaries: Ecosystem modeling and restoration. In Adey, W. H. and Loveland, K., editors, *Dynamic Aquaria (Third Edition)*, pages 405–441. Academic Press, London, third edition edition.

Allen, G. P. and Castaing, P. (1973). Suspended sediment transport from the gironde estuary (france) onto the adjacent continental shelf. *Marine Geology*, 14(5):47–53.

Allen, J. (1978). Computational models for dune time-lag: calculations using stein's rule for dune height. *Sedimentary Geology*, 20:165–216.

Arora, C., Kumar, B. P., and Narayana, A. (2010). Influence of particle shape on drag coefficient for commonly occuring sandy particles in coastal areas. *The International Journal of Ocean and Climate Systems*, 1(2):99–112.

Ashley, G. M. (1990). Classification of large-scale subaqueous bedforms; a new look at an old problem. *Journal of Sedimentary Research*, 60(1):160–172.

Auguste, C., Marsh, P., Nader, J.-R., Penesis, I., and Cossu, R. (2021). Modelling morphological changes and migration of large sand waves in a very energetic tidal environment: Banks strait, australia. *Energies*, 14(13).

Baar, A. W., de Smit, J., Uijttewaal, W. S. J., and Kleinhans, M. G. (2018). Sediment transport of fine sand to fine gravel on transverse bed slopes in rotating annular flume experiments. *Water Resources Research*, 54(1):19–45.

BAGNOLD, R. (1956). The flow of cohesionless grains in fluids. *PHILOSOPHICAL TRANSACTIONS OF THE ROYAL SOCIETY OF LONDON SERIES A-MATHEMATICAL AND PHYSICAL SCIENCES*, 249(964):235–&.

Berne, S., Castaing, P., Le Drezen, E., and Lericolais, G. (1993). Morphology, internal structure, and reversal of asymmetry of large subtidal dunes in the entrance to Gironde Estuary (France). *Journal of Sedimentary Research*, 63(5):780–793.

Besio, G., Blondeaux, P., Brocchini, M., and Vittori, G. (2004). On the modeling of sand wave migration. *Journal of Geophysical Research: Oceans.*, 109:1–13.

Best, J. (2005). The fluid dynamics of river dunes: A review and some future research directions. *Journal of Geophysical Research: Earth Surface*, 110(F4).

Bijker, R., Wilkens, J., and Hulscher, S. J. M. H. (1998). *Sandwaves: where and why.* International Society of Offshore and Polar Engineers, United States.

Billy, J., Chaumillon, E., Féniès, H., and Poirier, C. (2012). Tidal and fluvial controls on the morphological evolution of a lobate estuarine tidal bar: The plassac tidal bar in the gironde estuary (france). *Geomorphology*, 169-170:86–97.

Blom, A., Ribberink, J. S., and de Vriend, H. J. (2003). Vertical sorting in bed forms: Flume experiments with a natural and a trimodal sediment mixture. *Water Resources Research*, 39(2).

Bo, T., Ralston, D. K., Kranenburg, W. M., Geyer, W. R., and Traykovski, P. (2021). High and variable drag in a sinuous estuary with intermittent stratification. *Journal of Geophysical Research: Oceans*, 126(10):e2021JC017327. e2021JC017327 2021JC017327.

Boehlich, M. J. and Strotmann, T. (2008). The elbe estuary. *Die Küste*, pages 288–306.

Bokuniewicz, H., Gordon, R., and Kastens, K. (1977). From and migration of sand waves in a large estuary, long island sound. *Marine Geology*, 24(3):185–199.

Bradley, R. W. and Venditti, J. G. (2017). Reevaluating dune scaling relations. *Earth-Science Reviews*, 165:356–376.

Campmans, G. H. P., Roos, P. C., de Vriend, H. J., and Hulscher, S. J. M. H. (2017). Modeling the influence of storms on sand wave formation: A linear stability approach. *Continental Shelf Research*, 137:103–116.

Carling, P. (1999). Subaqueous gravel dunes. *Journal of Sedimentary Research - J SEDIMENT RES*, 69.

Chernetsky, A. S., Schuttelaars, H. M., and Talke, S. A. (2010). The effect of tidal asymmetry and temporal settling lag on sediment trapping in tidal estuaries. *Ocean Dynamics*, 60:1219–1241.

Colling, A., Brown, E., Wright, J. B. (John B.), ., Park, D., and Team, O. U. O. C. (1999). *Waves, tides and shallow-water processes*. Oxford : Butterworth-Heinemann ; Milton Keynes : Open University, 2nd ed. / revised by john wright, angela colling and dave park edition. Published in association with The Open University.

Dai, Z.-j., Fagherazzi, S., Mei, X., Chen, J., and Meng, Y. (2016). Linking the infilling of the north branch in the changjiang (yangtze) estuary to anthropogenic activities from 1958 to 2013. *Marine Geology*, 379.

Dalrymple, R. W. and Choi, K. (2007). Morphologic and facies trends through the fluvial–marine transition in tide-dominated depositional systems: A schematic framework for environmental and sequence-stratigraphic interpretation. *Earth-Science Reviews*, 81(3):135–174.

Damen, J. M., van Dijk, T. A. G. P., and Hulscher, S. J. M. H. (2018). Spatially varying environmental properties controlling observed sand wave morphology. *JOURNAL OF GEOPHYSICAL RESEARCH-EARTH SURFACE*, 123(2):262–280.

Damme, S. V., Struyf, E., Maris, T., Ysebaert, T., Dehairs, F., Tackx, M., Heip, C., and Meire, P. (2005). Spatial and temporal patterns of water quality along the estuarine salinity gradient of the scheldt estuary (belgium and the netherlands): results of an integrated monitoring approach. *Hydrobiologia*, 540(1):29–45.

de Jonge, V. N., Schuttelaars, H. M., van Beusekom, J. E., Talke, S. A., and de Swart, H. E. (2014). The influence of channel deepening on estuarine turbidity levels and dynamics, as exemplified by the ems estuary. *Estuarine, Coastal and Shelf Science*, 139:46–59.

Dronkers, J. (1986). Tidal asymmetry and estuarine morphology. *Netherlands Journal of Sea Research*, 20(2):117–131.

Francken, F., Wartel, S., Parker, R., and Taverniers, E. (2004). Factors influencing subaqueous dunes in the scheldt estuary. *Geo-Marine Letters*, 24:14–21.

Geyer, W. R. and MacCready, P. (2014). The estuarine circulation. *Annual Review of Fluid Mechanics*, 46(1):175–197.

Grabemann, I., Uncles, R., Krause, G., and Stephens, J. (1997). Behaviour of turbidity maxima in the tamar (u.k.) and weser (f.r.g.) estuaries. *Estuarine, Coastal and Shelf Science*, 45(2):235–246.

Guo, L., Wang, Z. B., Townend, I., and He, Q. (2019). Quantification of tidal asymmetry and its nonstationary variations. *Journal of Geophysical Research: Oceans*, 124(1):773–787.

Gurnell, A. (2014). Plants as river system engineers. *Earth Surface Processes and Landforms*, 39(1):4–25.

Herrling, G., Becker, M., Lefebvre, A., Zorndt, A., Krämer, K., and Winter, C. (2021). The effect of asymmetric dune roughness on tidal asymmetry in the weser estuary. *Earth Surface Processes and Landforms*, 46(11):2211–2228.

Hu, K., Ding, P., Wang, Z., and Yang, S. (2009). A 2d/3d hydrodynamic and sediment transport model for the yangtze estuary, china. *Journal of Marine Systems*, 77(1):114–136.

Hulscher, S. (1996). Tidal-induced large-scale regular bed form patterns in a three-dimensional shallow water model. *Journal of geophysical research : Oceans*, 101(C9):20727–20744.

Hulscher, S., de Swart, H., and de Vriend, H. (1993). The generation of offshore tidal sand banks and sand waves. *Continental shelf research*, 13((11)):1183–1204.

Hulscher, S. J. M. H. and Dohmen-Janssen, C. M. (2005). Introduction to special section on marine sand wave and river dune dynamics. *Journal of Geophysical Research: Earth Surface*, 110(F4).

Kennish, M. J. (2002). Environmental threats and environmental future of estuaries. *Environmental Conservation*, 29(1):78–107.

Lange, D., Müller, H., Piechotta, F., and Schuber, R. (2008). The weser estuary. *Die Küste*, pages 275–287.

Leuven, J. R. F. W., Pierik, H. J., Vegt, M. v. d., Bouma, T. J., and Kleinhans, M. G. (2019). Sea-level-rise-induced threats depend on the size of tide-influenced estuaries worldwide. *Nature Climate Change*, 9(12):986–992.

Li, C., Valle-Levinson, A., Atkinson, L. P., Wong, K. C., and Lwiza, K. M. M. (2004). Estimation of drag coefficient in james river estuary using tidal velocity data from a vessel-towed adcp. *Journal of Geophysical Research: Oceans*, 109(C3).

Lokin, L. R., Warmink, J. J., Bomers, A., and Hulscher, S. J. M. H. (2022). River dune dynamics during low flows. *GEOPHYSICAL RESEARCH LETTERS*, 49(8).

Lu, H., Gu, F., Qi, D., Chen, X., and Wang, Y. (2019). Investigating Near-Bottom Hydrodynamic Processes in the Yangtze River Estuary Using In Situ Measurements. *Journal of Coastal Research*, 35(4):805 – 813.

Lyu, H. and Zhu, J. (2018). Impact of the bottom drag coefficient on saltwater intrusion in the extremely shallow estuary. *Journal of Hydrology*, 557:838–850.

Maas, L. and Haren, J. (1987). Observations on the vertical structure of tidal and inertial currents in the central north sea. *Journal of Marine Research*, 45:293–318.

McCave, I. (1971). Sand waves in the north sea off the coast of holland. *Marine Geology*, 10:199–225.

Muurman, S. (2021). Data analysis of estuarine dunes: Linking estuarine sand dune characteristics to environmental parameters.

Nemeth, A. A., Hulscher, S. J. M. H., and de Vriend, H. J. (2002). Modelling sand wave migration in shallow shelf seas. *Continental Shelf Research*, 22:2795–2806.

Ong, J.-E., Gong, W.-K., and Uncles, R. (1994). Transverse structure of semi-diurnal currents over a cross-section of the merbok estuary, malaysia. *Estuarine, Coastal and Shelf Science*, 38:283–290.

Paarlberg, A., Dohmen-Janssen, C., Hulscher, S., van den Berg, J., and Termes, A. (2006). Modelling morphodynamic evolution of river dunes. In Ferreira, R., editor, *Proceedings of River Flow 2006, 6-8 September 2006, Lisbon, Portugal*, pages 969–978, United Kingdom. Taylor & Francis.

Papenmeier, S. (2012). *Properties and dynamics of suspended load and near-bed fine cohesive sediments in highly impacted estuaries. Case studies from the Weser, Ems and Elbe estuaries (Germany)*. PhD thesis, Christian-Albrechts Universität.

Papenmeier, S., Schrottke, K., and Bartholomä, A. (2014). Over time and space changing characteristics of estuarine suspended particles in the german weser and elbe estuaries. *Journal of Sea Research*, 85:104–115.

Prandle, D. (1985). On salinity regimes and the vertical structure of residual flows in narrow tidal estuaries. *Estuarine, Coastal and Shelf Science*, 20(5):615–635.

Schramkowski, G. P. and de Swart, H. E. (2002). Morphodynamic equilibrium in straight tidal channels: Combined effects of the coriolis force and external overtides. *Journal of Geophysical Research: Oceans*, 107(C12):20–1–20–17.

Schrottke, K., Becker, M., Bartholomä, A., Flemming, B. W., and Hebbeln, D. (2006). Fluid mud dynamics in the weser estuary turbidity zone tracked by high-resolution side-scan sonar and parametric sub-bottom profiler. *Geo-Marine Letters*, 26(3):185–198.

Shuwei, Z., Cheng, H., Wu, S., Liu, G., Lu, X., and Xu, W. (2016). Discovery and implications of catenary-bead subaqueous dunes. *Science China Earth Sciences*, 59:495–502.

Sistermans, P. and Nieuwenhuis, O. (2021). *WESTERN SCHELDT ESTUARY (THE NETHERLANDS)*. http://www.eurosion.org.

Terwindt, J. (1971). Sand waves in the southern bight of the north sea. *Marine Geology*, 10:51–67.

Ullman, D. S. and Wilson, R. E. (1998). Model parameter estimation from data assimilation modeling: Temporal and spatial variability of the bottom drag coefficient. *Journal of Geophysical Research: Oceans*, 103(C3):5531–5549.

van der Sande, W. M., Roos, P. C., Gerkema, T., and Hulscher, S. J. (2021a). Gravitational circulation as driver of upstream migration of estuarine sand dunes. *Geophysical research letters*, 48(14).

van der Sande, W. M., Roos, P. C., Gerkema, T., and Hulscher, S. J. (2021b). Matlab code for "Gravitational circulation as driver of upstream migration of estuarine sand dunes".

van der Sande, W. M., Roos, P. C., and Hulscher, S. J. (2019). Investigating idealized modelling of estuarine sand waves. In *MARID VI, Marine and River dunes dynamics 2019, Book of Abstracts*, pages 231–234. MARID VI, Marine and River Dune Dynamics 2019, MARID VI ; Conference date: 01-04-2019 Through 03-04-2019.

van Dijk, T. A. G. P. and Kleinhans, M. G. (2005). Processes controlling the dynamics of compound sand waves in the north sea, netherlands. *Journal of Geophysical Research: Earth Surface*, 110(F4).

van Maanen, B. and Sottolichio, A. (2018). Hydro- and sediment dynamics in the gironde estuary (france): Sensitivity to seasonal variations in river inflow and sea level rise. *Continental Shelf Research*, 165:37–50.

van Rijn, L. C. (1993). *principles of sediment transport in rivers, estuaries and coastal seas*. AQUA PUBLICATIONS.

Vandenbruwaene, W., Plancke, Y., Verwaest, T., and Mostaert, F. (2013). *Interestuarine comparison: Hydro-geomorphology: Hydro- and geomorphodynamics of the TIDE estuaries Scheldt, Elbe, Weser and Humber.* Flanders Hydraulics Research.

Vandenbruwaene, W., Vos, G., Plancke, Y., and Mostaert, F. (2012). *Werkgroep O&M - Projectgroep Veiligheid en Toegankelijkheid: Onderzoek naar de morfologie op meso-schaal ter hoogte van stortlocaties.Versie 3.0. WL Rapporten, 791_10a.* Waterbouwkundig Laboratorium Antwerpen, België.

Vittori, G. and Blondeaux, P. (2020). River dunes and tidal sand waves: Are they generated by the same physical mechanism? *WATER RESOURCES RESEARCH*, 56(5).

Wan, Y., Gu, F., Wu, H., and Roelvink, D. J. (2014). Hydrodynamic evolutions at the yangtze estuary from 1998 to 2009. *Applied Ocean Research*, 47:291–302.

Warmink, J. J., Dohmen-Janssen, C. M., Lansink, J., Naqshband, S., van Duin, O. J. M., Paarlberg, A. J., Termes, P., and Hulscher, S. J. M. H. (2014). Understanding river dune splitting through flume experiments and analysis of a dune evolution model. *EARTH SURFACE PROCESSES AND LANDFORMS*, 39(9):1208–1220.

Wei, X., Schramkowski, G. P., and Schuttelaars, H. M. (2016). Salt dynamics in well-mixed estuaries: Importance of advection by tides. *Journal of Physical Oceanography*, 46(5):1457 – 1475.

Weihua, L., Cheng, H.-Q., Jiufa, L., and Ping, D. (2008). Temporal and spatial changes of dunes in the changjiang (yangtze) estuary, china. *Estuarine, Coastal and Shelf Science*, 77(1):169 – 174.

Wienberg, C. and Hebbeln, D. (2005). Impact of dumped sediments on subaqueous dunes, outer weser estuary, german bight, southeastern north sea. *Geo-Marine Letters*, 25:43–53.

Wiesemann, J.-U., Mewis, P., and Zanke, U. C. E. (2006). Downslope transport (transverse sediment transport).

Wilbers, A. and Ten Brinke, W. (2003). The response of subaqueous dunes to floods in sand and gravel bed reaches of the dutch rhine. *Sedimentology*, 50(6):1013–1034.

Wu, J. X., Wang, Y., and Cheng, H. (2009). Bedforms and bed material transport pathways in the changjiang (yangtze) estuary. *Geomorphology*, 104:175–184.

Wu, S., Cheng, H., Xu, Y., Li, J., and Zheng, S. (2016a). Decadal changes in bathymetry of the yangtze river estuary: Human impacts and potential saltwater intrusion. *Estuarine, Coastal and Shelf Science*, 182:158–169.

Wu, S., Cheng, H., Xu, Y. J., Li, J., Zheng, S., and Xu, W. (2016b). Riverbed micromorphology of the yangtze river estuary, china. *Water*, 8(5).

Zomer, J. Y., Naqshband, S., Vermeulen, B., and Hoitink, A. J. F. (2021). Rapidly migrating secondary bedforms can persist on the lee of slowly migrating primary river dunes. *Journal of Geophysical Research: Earth Surface*, 126(3):e2020JF005918. e2020JF005918 2020JF005918.

Zorndt, A. C., Wurpts, A., Schlurmann, T., Ohle, N., and Strotmann, T. (2011). Dune migration and sand transport rates in tidal estuaries: The example of the river elbe. *Coastal Engineering Proceedings*, 1(32):sediment.38.

Appendices

A. Surface calculation

This appendix explains the calculation of the surface area of a cross-section surface of the estuaries used in paragraph 3.3

A.1. Elbe estuary

Boehlich and Strotmann (2008) describes the cross-section area of the tidal part of the Elbe based on the Elbe-Km. The maximum cross-sectional area is 5.1*10 ^{4} m^2 for mean sea level, close to the estuary mouth. This maximum cross-section increases for mean sea level+1.5 meters to 6.0*10^4 m^2 . The cross-sectional area decreases to less than 1.0*10^4 m^2 at Hamburg. An estimate of 3.2*10^4 m^2 represents the area close to the sea. An area of 2.0*10^4 m^2 represents the area halfway in the estuary(Elbe km 660-685). We use the cross-section close to the sea to calculate the river discharge velocity.

A.2. Gironde estuary

The Gironde estuary cross-section surface is estimated to be 8.0*10^4 m^2 based on the estimation of van der Sande et al. (2021a).

A.3. Weser estuary

Lange et al. (2008) describes the cross-sectional area along the lower Wesser. The maximum cross-section is 9.5*10^3 m^2 found at km 65 (close to Bremshaven), the minimum cross-section is 2.0*10 ^{3} m^2 at Oslebshausen.

A.4. Western Scheldt estuary

Muurman (2021) describes three bed level profiles for the Western Scheldt, located at Vlissingen, Terneuzen and Borssele. The cross-section of Vlissingen has an average depth of 22.5 meters depth and a width of 1200 meters. So at a cross-section at Vlissingen is 2.7*10^4 m^2. The cross-section at Terneuzen has a maximum depth of 34 meters and an average area of 2.42*10^4 m^2. An estimate for the cross-section area of Borssele is 3.0*10^4 m^2. So the average cross-section calculated is 2.7*10^4 m^2

A.5. Yangtze estuary

The Yangtze River splits in the estuary into several channels. Therefore the sum of the different cross-sections is used to describe the total cross-section. As in Figure 28 shows. The estuary consists of a North and South Branch. The South Branch splits in the North and South Channel. The southern channel splits more down streams in the north and South Passage. The total cross-section area consists of the sum of the cross-sections of the North Branch and the North and South channel.

The North Branch has a depth of mean depth that decreases from 5.85 meters in 1958 to 3.14 meters in 2003 and has a mean of 3.86 meters over the period 1958-2013 (Dai et al., 2016). The cross-section calculation uses the time-averaged mean water depth. The width of the North Branch varies from 1 km upstream to 8 km at the mouth. The upstream area has an estimated mean width of 1.8 km. The width is 3.5 km (at road G40), close to cross-sections NC1 and SC1 in the North Branch (Wu et al., 2016a).The cross-section area varies over length. In the upstream North Branch, this is $6.9 * 10^3$ m^2 and $1.4 * 10^4$ m^2 area close to the G40 road. Wu et al. (2016a) describes several cross-sections of both the North and South Channel. The first cross-section of the South Channel is $6.5*\ 10^4$ m^2. The first cross-section of the North Channel in this paper is approximately $7.0*10^4$ m^2. So the sum of the three different channels is $1.5*10^5$ m^2

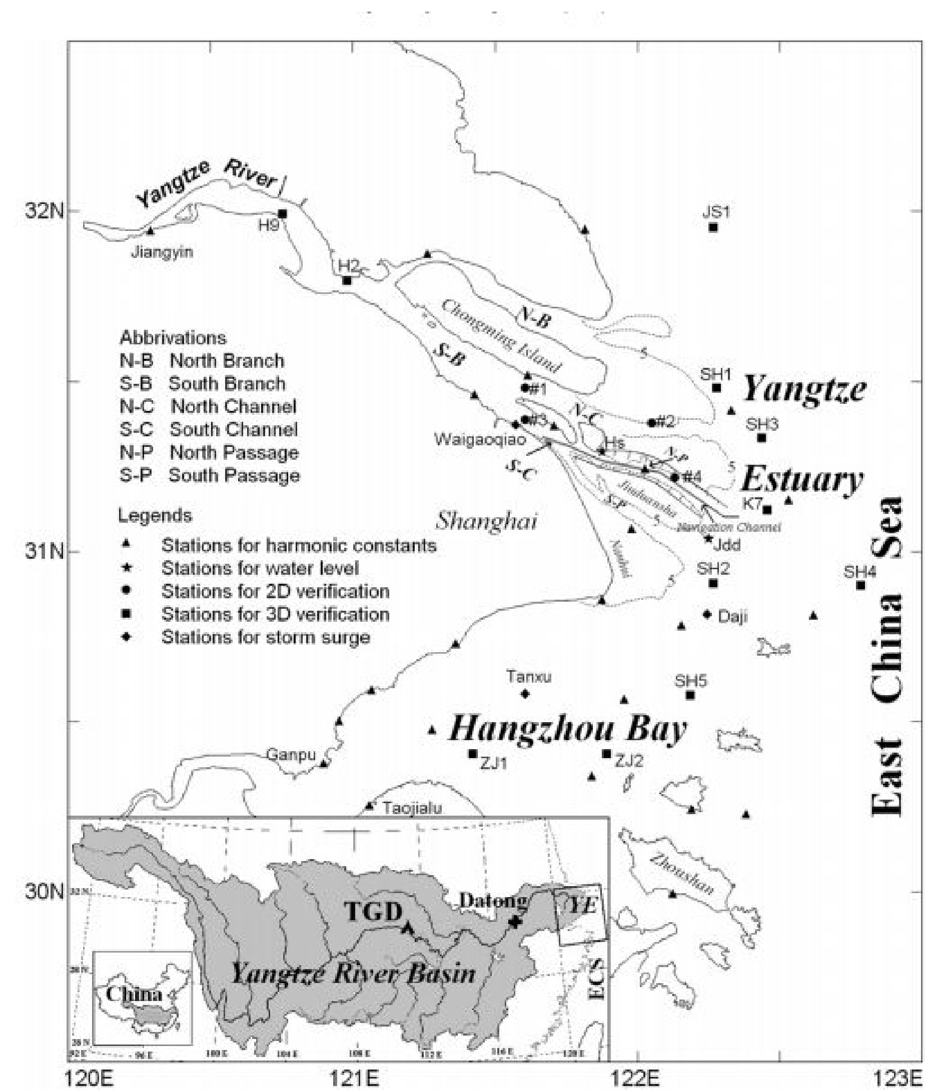

Figure 28: Overview of Yangtze Estuary Hu et al. (2009)